Nodal signaling has dual roles in fate specification and directed migration during germ layer segregation

Zairan Liu[1,2], Stephanie Woo[3], Orion D. Weiner[1,2*]

[1] Cardiovascular Research Institute, University of California, San Francisco, San Francisco, CA 94158

[2] Department of Biochemistry and Biophysics, University of California, San Francisco, San Francisco, CA 94158

[3] School of Natural Sciences, University of California, Merced, CA 95343, USA

* Lead Contact, correspondence: orion.weiner@ucsf.edu (O.D.W.)

Key Words

Nodal signaling Ingression Endoderm Germ layer segregation Zebrafish gastrulation

Summary Statement

Autocrine Nodal signaling is necessary and sufficient to drive sorting of ectopic endodermal cells to the zebrafish inner layer.

Abstract

During gastrulation, endodermal cells actively migrate to the interior of the embryo, but the signals that initiate and coordinate this migration are poorly understood. By transplanting ectopically-induced endodermal cells far from the normal location of endoderm specification, we identified the inputs that drive internalization without the confounding influences of fate specification and global morphogenic movements. We find that Nodal signaling triggers an autocrine circuit for initiating endodermal internalization. Activation of the Nodal receptor directs endodermal specification through *sox32* and also induces expression of more Nodal ligands. These ligands act in an autocrine fashion to initiate endodermal cell sorting. Our work defines an "AND" gate consisting of *sox32*-dependent endodermal specification and Nodal ligand reception controlling endodermal cell sorting to the inner layer of the embryo at the onset of gastrulation.

Introduction

Gastrulation is central to animal development and involves the specification of three different germ layers (endoderm, mesoderm, and ectoderm) and their segregation to different locations in the embryo (Wolpert 1992). In contrast to the mechanisms underlying cell fate specification, the mechanisms used to drive segregation of the three germ layers are much less well understood. In this work, we focus on endodermal cells, which are initially specified on the surface of the embryo but must segregate to the interior, where they give rise to the gut and associated tissues. Endoderm migration is crucial for the formation of the gut tube and digestive tract across the animal kingdom. The in-folding of surface blastoderm cells to form the endoderm is well-documented in a wide range of species (Stern 2004; Wolpert 1992) . However, it has been experimentally difficult to separate the initiation of migration events from cell fate specification. Thus, the molecular logic of the cell internalization, including which signals trigger this migration and how cell fate and migration are related, still remain unclear.

Several models have been proposed for how the germ layers segregate during embryogenesis. Most prominently, the differential adhesion hypothesis proposed that differences in intercellular adhesion among the different germ layers drives sorting (Steinberg 1962). However, although differential adhesion and cortex tension have been observed *in vitro*, *in vivo* measurements of tissue surface tension were indistinguishable among the three germ layers. Thus, differential adhesion is unlikely to fully account for the ability of the germ layers to sort in the embryo (Krieg et al. 2008; Maître et al. 2012; Krens et al. 2017).

Previous studies have shown that directed cell migration appears to be the driving force for endoderm segregation *in vivo* for zebrafish (Montero et al. 2005; Krens et al. 2017; Giger and David 2017). At the onset of zebrafish gastrulation, the blastoderm consists of several thousand cells positioned above the yolk cell. Internalization begins on the dorsal side where inward-moving cells form the hypoblast (mesoderm and endoderm) in contrast to the cells remaining on the outside as epiblast (ectoderm) (R. M. Warga and Kimmel 1990). A germ ring forms at the boundary of hypoblast and epiblast and the embryonic shield is formed on the dorsal side of the margin. Early dye labeling experiments showed that cells relocate to deeper levels within the germ ring by inverting their order relative to the margin as they internalize (Kimmel and Warga 1987). Initially, an involution model was proposed to describe the population flow as a cellular sheet (Lewis 1985). Later, time-lapse tracking showed that individual cells within the germ ring transiently move out of the epiblast and relocate into the hypoblast (D'Amico and Cooper 1997;

Concha and Adams 1998). More recent studies have shown such cells extend protrusions inward and exhibit active directed migration (Montero et al. 2005; Krens et al. 2017; Giger and David 2017)

Nodal, as a member of the TGF-β superfamily, is essential for germ layer patterning in zebrafish. Nodal ligands are expressed at the margin and yolk syncytial layer (YSL) during the blastula stage, where it forms a morphogen gradient (Chen and Schier 2001; Dougan et al. 2003). The signaling pathway is activated by Nodal binding to a type II TGF-β receptor, inducing interaction with an EGF-CFC co-receptor, One-eyed-pinhead (Tdgf1), and the type I TGF-β receptor, Acvr1ba (Weng and Stemple 2003; Gritsman et al. 1999; Aoki, Mathieu, et al. 2002). Subsequent phosphorylation of the transcription factors Smad2 and Smad3 facilitates the formation, together with Smad4, of a Smad complex which translocates into the nucleus to regulate the expression of target genes (Weng and Stemple 2003; Jia et al. 2008). One of the key downstream targets is the *sox32*, which plays an essential cell-autonomous role in endoderm formation (Kikuchi et al. 2001).

Compared to endoderm specification, the signals which initiate and direct endoderm migration are not as well understood. From previous studies, it is known that endodermal cells initially undergo random walk migration but switch to convergence movements at mid-gastrulation (Pézeron et al. 2008). Endodermal migration is also regulated by chemokine signaling downstream of the Nodal pathway (Nair and Schilling 2008; Mizoguchi et al. 2008). We recently demonstrated that Nodal signaling regulates endodermal cell motility and actin dynamics via Rac1 and Prex1 (Woo et al. 2012). However, it is not known whether these migration patterns arise due to endodermal cell fate alone or whether additional cues in their morphogenic field are required.

Here we utilized an *in vivo* system to study germ layer segregation in zebrafish embryos. In the early zebrafish embryo, an initially mixed mesendodermal population ultimately resolves into distinct mesodermal and endodermal cell layers, but these complex morphogenetic movements occur simultaneously with fate specification (Ho 1992). To disentangle the endodermal specification program from the migration program, we used a constitutively-active version of the Nodal receptor, *acvr1ba**, to predispose cells into an endodermal fate (Renucci, Lemarchandel, and Rosa 1996; Aoki, Mathieu, et al. 2002; David and Rosa 2001). By transplanting these ectopically-induced endodermal cells into the animal pole of the embryo, we removed them from

the endogenous signals that normally orchestrate endodermal development as well as the effects of nearby ingressing cells. We found that these ectopically-introduced endodermal cells do not take the normal path of endogenous endoderm migration by internalizing at the germ ring; instead they radially ingress into the inner layer. Nodal signaling is necessary and sufficient to initiate this process, and the ectopic endodermal cells (but not the surrounding cells) need to receive the Nodal ligand in an autocrine fashion to trigger ingression. Our results suggest that Nodal signaling plays dual roles in specifying endodermal fate and initiating the sorting of these cells to the interior of the embryo. As these migration events are not observed for *in vitro* culture conditions, this *in vivo* approach for endodermal sorting should be a powerful system for continued dissection of the logic of germ layer segregation during gastrulation.

Results

*acvr1ba**-induced endodermal cells ingress into the inner layer of the embryo when placed near the animal pole

To determine the requirements for initiating and directing endoderm migration, we developed a cell transplantation model that allowed us to directly query endodermal sorting while disentangling the endodermal specification program from the migration program. We generated ectopic endodermal cells by expression of the constitutively activated Nodal receptor *acvr1ba*.* We then transplanted these cells (**Fig. 1A**) into the animal pole of a wild-type host embryo, far from the marginal location of endogenous endodermal cells, and determined whether these misplaced ectopic endodermal cells could sort into the correct endodermal layer. (**Fig. 1B**). First, ectopic endoderm production by *acvr1ba** was confirmed by qPCR analysis of *sox17* and *sox32* expression (**Fig. S1A**), markers for endodermal cell fate (Kikuchi et al. 2001, 17; Shivdasani 2002). Although Nodal signaling can also induce mesoderm fate (Peyriéras, Strähle, and Rosa 1998; Aoki, Mathieu, et al. 2002), we found that *acvr1ba** expression upregulated the mesodermal markers *gsc* and ntl to a lesser extent that *sox17* and *sox32* (**Fig. S1B**), demonstrating that *acvr1ba**-expressing cells are biased to an endoderm fate. Next, we found that, after transplantation to the animal pole, these ectopically introduced endodermal cells accumulated in endoderm-derived tissue by preferentially migrating to the correct endodermal layer (**Fig. 1B-E**). When induced endodermal cells were transplanted together with non-endodermal cells (**Fig. 1F**), these cell types separated into two layers from an originally mixed population (**Fig. 1G, Movie S1**). Visualizing the migration path of these cells by time-lapse microscopy showed that induced endodermal cells did not move towards the margin and then

involute to form endodermal layer (the normal path of endogenous endoderm migration); instead, they radially ingressed into the inner layer (**Fig. 1G**), consistent with a recent report (Giger and David 2017). Additional single-cell tracking analysis revealed that the trajectories of transplanted cells did not exhibit random walk or sample both inward and outward directions; instead, the ingression was highly unidirectional (**Fig. 1H, Movie S2**). These data indicate that endodermal cells produced by *acvr1ba** expression can initiate ingression if placed ectopically via highly polarized and unidirectional migration.

Sorting of ectopic endodermal cells requires both Nodal signaling and *sox32*-dependent endoderm specification

We next sought to define the molecular logic of ectopic endodermal cell sorting. In addition to expressing the constitutively activated Acvr1ba* receptor, ectopic endodermal cells can also be produced by overexpression of the transcription factor Sox32, a target of Nodal signaling (Dickmeis et al. 2001; Kikuchi et al. 2001; Sakaguchi, Kuroiwa, and Takeda 2001, 32). However, previous work suggested that, unlike Acvr1ba* expression, overexpression of *sox32* is not sufficient to drive the sorting process (Kikuchi et al. 2001). We too observed that cells overexpressing *sox32* could preferentially segregate to endoderm-derived tissues when placed near the dorsal margin but not when transplanted to the animal pole (**Fig. 2A-B, S2**).

Notably, this means that these two different means of generating endodermal cells (*acvr1ba* vs sox32*) are not equivalent in their ability to drive internalization movements when transplanted far from the normal endodermal domain (**Fig. 2C**); only *acvr1ba** induced endodermal cells are capable of ingression when placed at the animal pole. These data suggest that Nodal signaling initiates endodermal sorting in addition to specifying endodermal fate. *acvr1ba** likely activates additional pathways that are absent when *sox32* is overexpressed, thus allowing cells to sort regardless of the location within the embryo. In contrast, cells overexpressing *sox32* may require extrinsic factors present at the margin to activate these additional “sorting” pathways, explaining why they can only sort in regions close to the margin (Kikuchi et al. 2001). These observations suggest that the triggering of sorting involves an “AND” gate consisting of *sox32*-dependent endodermal specification and additional signaling downstream of *acvr1ba** (**Fig. 2D**).

To confirm the necessity of *sox32*-dependent arm of the putative AND gate, we injected *acvr1ba**-induced endodermal cells with *sox32* MO, which blocks the transcriptional program that initiates endodermal specification (Sakaguchi, Kuroiwa, and Takeda 2001; Dickmeis et al.

2001) (Fig. Sx). We found that these cells lost the ability to ingress into the inner layer of the embryo after transplantation to the animal pole of a wild-type host (**Fig. 2G, H**). Single cell tracking revealed that morpholino against *sox32* (**Fig S5**) inhibits the ability of *acvr1ba** cells to migrate to the interior of the embryo. These results suggest that both autocrine production of Nodal ligands and *sox32*-dependent endodermal specification are necessary to trigger ectopic endodermal sorting.

To better understand the differences between these two methods of generating ectopic endoderm, we compared the signaling and transcriptional networks activated by *acvr1ba* and *sox32*. A recent report (Giger and David 2017) suggested that N-cadherin (cdh2) expression triggers endoderm ingression. However, we found that both *acvr1ba** and *sox32* overexpression induced cdh2 expression (**Fig. S1C**) to similar extents. This suggests that N-cadherin expression alone does not account for the difference of ingression capability between these two types of endodermal cells.

Nodal ligand expression is necessary to trigger the sorting of ectopic endodermal cells

Nodal signaling through *acvr1ba*, but not *sox32* alone, is capable of inducing expression of Nodal ligands *ndr1* and *ndr2* (Chan et al. 2009; Feldman et al. 1998; Dougan et al. 2003). In wild-type embryos, these ligands are expressed highest near the margin, which could explain the observation that *sox32*-induced endodermal cells only sort in this location. In contrast, the autocrine production of Nodal ligands downstream of *acvr1ba** could enable these cells to sort regardless of location in the embryo. To confirm that *ndr1/2* is secreted by *acvr1ba**-expressing cells but not by cells expressing *sox32*- alone, we quantified the *ndr1/2* expression profile under all experimental conditions (**Fig. S3**). When transplanted to WT embryos, we saw a 2-3 fold increase of *ndr1/2* expression in *acvr1ba**-expressing cells compared to the *sox32*-expressing cells. However, this is likely an underestimate of the difference in nodal ligand expression induced by *acvr1ba** or *sox32* expression due to the presence of maternally deposited *ndr1/2* in the host embryo that can also trigger a Nodal positive feedback loop. To address this complication, we expressed *acvr1ba** and *sox32* in maternal-zygotic (MZ) *tdgf1* mutant embryos, which lack sufficient Nodal signaling (Gritsman et al. 1999) **(Fig. S3B)**. In this background, we found that *acvr1ba** expression increased *ndr1* expression 25-fold higher than *sox32* expression. Finally, injection of *ndr1/2* mRNA increased the expression of *ndr1/2* in *sox32*-expressing cells to similar levels seen in *acvr1ba**-expressing cells **(Fig. S3C)**. Taken together, these data confirm that *acvrb1a**, but not *sox32*, induces nodal ligand expression.

Next, we sought to test whether the excess production of Nodal ligands is the driver of ingression. We first examined the necessity of Nodal ligand expression for endodermal sorting by using morpholinos to knockdown *ndr1* and *ndr2* in the *acvr1ba**-induced endodermal cells, which were then transplanted into the animal pole of wild-type embryos (**Fig. 2E**). We verified the functionality of the morpholinos by demonstrating the inhibition of *sox17* expression (**Fig. S4**). At 20 hpf, while cells expressing *acvr1ba** only preferentially localized to endodermal tissues such as the pharynx, the *acvr1ba** cells with *ndr1* and *ndr2* MO knockdown primarily localized in non-endodermal tissue, particularly in the head region (**Fig. 2F, H**). Single cell tracking revealed that the *acvr1ba** cells with *ndr1* and *ndr2* MO remain in the ectoderm and move near the surface of the embryo (**Fig. 2I**). Notably, the failure to ingress caused by knockdown of *ndr1* and *ndr2* is unlikely to be due to effects on endoderm specification as cells maintained endoderm identity as assessed by *Tg(sox17:GFP)* reporter expression (**Fig. 2J-K**).

To further test if *ndr1/2* secretion is necessary for sorting, we analyzed the internalization dynamics of *acvr1ba**- or *sox32*-overexpressing cells in host embryos injected with *ndr1/2* MO. After transplantation into the margin of a *ndr1/2*-depleted host, *acvr1ba**-expressing cells localized to the endoderm-derived tissue (**Fig. S6**). In contrast to our animal pole transplantation experiments, *sox32*-overexpressing cells transplanted to the margin of *ndr1/2*-depleted hosts were able to contribute to both endoderm and ectoderm-derived tissues, although the extent of endoderm contribution significantly less compared to *acvr1ba** cells (**Fig. S6**). Because there are still global morphogenesis movements happening at the margin of the host embryos, it is possible that some transplanted cells are internalized along with their host cell neighbors. Such community effects were previously observed for transplanted MZ *tdgf1* mutant cells that could initially internalize with their wild-type neighbors (Carmany-Rampey and Schier 2001). This might account for the increased percentage of endoderm contribution for marginally versus animal pole transplanted *sox32*-overexpressing cells.

In zebrafish, the two Nodal ligands Ndr1 and Ndr2 are known for their functional redundancy in inducing mesendoderm fate (Feldman et al. 1998; Erter, Solnica-Krezel, and Wright 1998; Jing et al. 2006). But it is not known whether they behave redundantly to induce ingression. To address this question, we performed transplantation experiments of *acvr1ba**-expressing cells with either *ndr1* MO or *ndr2* MO alone. Our results showed that neither *ndr1* MO or *ndr2* MO

abolished the ingression behavior of *acvr1ba**-expressing cells (**Fig. S7**). These data suggest that these nodal ligands act redundantly to support the ingression of *acvr1ba**-expressing cells.

Nodal ligand expression is sufficient to drive ingression of *sox32*-induced endodermal cells

Next, we investigated whether addition of Nodal ligands could trigger ectopic endodermal cell sorting in *sox32*-induced endodermal cells, which were not able to ingress into the inner layer when they are transplanted to the animal pole (**Fig. 3A**). To test this, we injected donor cells with mRNA for both *sox32* and Nodal ligands (*ndr1*, *ndr2*) prior to transplantation into wild-type embryos, using *acvr1ba**-induced endodermal cells as a positive control (**Fig. 3B**). When examined at the18-somite stage, *sox32*-injected cells also expressing Nodal ligands accumulated in endoderm-derived tissue significantly better than cells expressing *sox32* alone (**Fig. 3D, 3F-G**). These data indicate that the expression of Nodal ligands is sufficient to confer sorting ability in *sox32*-induced endodermal cells.

Can any cell expressing Nodal ligands sort to endodermal tissues, or do cells require both endodermal specification and Nodal ligand expression to support sorting? Because Nodal ligands themselves can drive endodermal fate (Chen and Schier 2001; David and Rosa 2001; Dougan et al. 2003), we addressed this question by overexpressing Nodal ligands in conjunction with *sox32* MO (**Fig. 3C**). We found that Nodal ligands cannot support sorting in the *sox32* MO background (**Fig. 3E, 3G**). These data suggest that Nodal ligands can only trigger sorting in conjunction with *sox32*-dependent endodermal specification. Together, our necessity and sufficiency experiments demonstrate that Nodal ligands and *sox32* constitute an “AND” gate to initiate internalization in the early embryo.

Sorting requires ectopic endodermal cells to receive Nodal signaling in an autocrine circuit

So far, we have shown that Nodal ligands production is necessary and sufficient to trigger the ingression-based cell sorting of ectopic endodermal cells. We next determined which cells are responding to the Nodal ligands to support sorting. The Nodal ligands could either be acting on the same endodermal cells that undergo sorting to form an autocrine circuit or on the surrounding cells in a paracrine circuit, possibly by orchestrating endodermal extrusion by the surrounding ectoderm (**Fig. 4A, 4B**). We pharmacologically blocked the autocrine reception of Nodal ligands by applying the Nodal receptor inhibitor SB505124 to *acvr1ba**-expressing cells. We found that 25-50 µM SB505124 inhibited endodermal cell fate specification, even in

embryos expressing *acvr1ba**, suggesting that this drug interfered with the signaling circuit upstream of *acvr1ba* (**Fig. S8A-C**). Following pharmacological Nodal inhibition, *acvr1ba**-expressing cells failed to internalize after being transplanted to the animal pole (**Fig. S8D**). To inhibit only the autocrine reception of the Nodal ligands while maintaining endodermal cell fate, we used the maternal-zygotic (MZ) *tdgf1* mutant to block Nodal signal reception; this mutant lacks the EGF-CFC co-receptor essential for the ability to respond to Nodal ligands (Gritsman et al. 1999). When we transplanted MZ *tdgf1* donor cells expressing *acvr1ba** into wild-type recipient hosts, the donor cells were incapable of ingressing into the inner layer of the host embryo and did not contribute to endoderm-derived tissue at the 18-somite stage (**Fig. 4C, 4F**). In contrast, when we injected *acvr1ba** into wild-type donor embryos and transplanted these cells into MZ *tdgf1* mutant host embryos, these transplanted cells still successfully ingressed into the inner layer, indicating that ectopic endodermal cells retained their ability to sort irrespective of the Nodal signaling state of the surrounding cells (**Fig. 4D, 4G**). Together, these results suggest that an autocrine circuit of Nodal ligand reception is required to support sorting of ectopic endodermal cells (**Fig. 4E**). Furthermore, because the MZ *tdgf1* mutant host embryos lack endogenous endoderm (Gritsman et al. 1999; David and Rosa 2001) but still supported ingression of ectopic endodermal cells, these experiments further suggest that signals released by endogenous endodermal cells are not required for ectopic endodermal cell sorting.

It is possible that blocking autocrine Nodal reception, either by drug treatment or loss of *tdgf1*, would also decrease ndr1/2 production and inhibit ingression. However, given that nuclear accumulation of Smad2 is not significantly different in *acvr1ba**-exressing embryos either with or without *ndr1/2* MO (**Fig. 2K**), a small decrease in Ndr1/2 production is unlikely to affect the magnitude of Nodal signal to an extent that would impact migration. Therefore, altered levels of Nodal activation do not account for the role of autocrine Ndr1/2 in endodermal internalization. More likely, autocrine reception of Nodal ligands may activate other signaling pathways downstream of *acvr1ba** as an input to the “AND” gate for sorting.

Nodal ligands initiate but do not guide the ingression of endodermal cells.

In our transplant experiments, we observed ectopic endodermal cells moving from the outer layer of the embryo radially to the inner layer, but we never observed cells moving in the opposite direction (i.e., extruded from the embryo). A recent study has shown that during normal gastrulation movements, endodermal cells at the margin extend polarized protrusions toward the yolk syncytial layer and appear to internalize by active migration(Giger and David 2017).

Therefore, we investigated whether ectopically placed endodermal cells similarly undergo active, directed migration to enter the interior of the embryo. To visualize actin dynamics in the ectopic endodermal cells during sorting, we expressed GFP-UTRN (Burkel, von Dassow, and Bement 2007), an actin reporter that we have previously used to analyze endodermal actin dynamics in zebrafish (Woo et al. 2012). We transplanted GFP-UTRN-labeled and *acvr1ba**-induced endodermal cells to the animal pole of wild-type hosts and imaged actin dynamics during ingression. We divided each single transplanted cell into two sectors, one facing towards the interior of the embryo and the other facing toward the embryo surface and then quantified the accumulation of actin in each sector. We observed a significant accumulation of actin in the interior-facing sector of ectopic endodermal cells as well as actin-based protrusions extending towards the interior of the embryo. Control transplanted cells not expressing *acvr1ba** lacked this polarity of actin enrichment and protrusions (**Fig. 5A-B**). In contrast, *acvr1ba**-expressing cells injected with *ndr1/2* MOs exhibit non-polarized protrusions, suggesting that protrusion generation may be normal but their orientation may be defective in the absence of *ndr1/2*. (**Fig. S9**). Together, these data indicate that an asymmetry in protrusion polarization in ectopic endodermal cells but not ones with *ndr1/2* knockdown. This indicates that *ndr1/2* are necessary to direct the actin-enriched protrusions, consistent with sorting based on active migration.

Which spatial cues are ectopic endodermal cells reading to achieve their directional migration? Such cues likely do not arise from the endogenous endodermal cells, as ectopic endoderm can still sort in an MZ *tdgf1* host that lacks endogenous endoderm (**Fig. 4E**). Might the endogenous Nodal gradient of the host embryo set the direction for ectopic endodermal cell migration? To investigate this hypothesis, we used *ndr1/2* MO to knock down endogenous Nodal ligands in host embryos (**Fig. 5C**). We transplanted *acvr1ba**-expressing donor cells to the animal pole and found that they maintained their ability to ingress into the inner layer of the embryo (**Fig. 5D-E**). These data suggest that the endogenous Nodal is not necessary to trigger the sorting behavior. Conversely, we saturated the endogenous Nodal gradient by overexpressing *ndr1* and *ndr2* ligands in the host embryo (**Fig. 5F-G**). As before, the *acvr1ba**-induced endodermal cells retained their ability to ingress into the inner layer (**Fig. 5H-I**) after transplantation. Together, these data suggest that although autocrine Nodal reception is essential for initiating internalization, neither the endogenous endodermal cells nor the endogenous Nodal ligands spatially direct ingression.

Discussion

In this work, we investigated the molecular signals that initiate the movement of endodermal cells from the surface to the interior of the embryo during zebrafish development. By leveraging the ability of ectopically-induced endodermal cells to sort to the endogenous endodermal domain, we dissected the molecular logic of sorting without the confounding influences of fate specification and global morphogenetic movements at the margin. Our work shows that an autocrine circuit of Nodal activated by *acvr1ba** is both necessary and sufficient to trigger internalization of endodermal cells (**Fig. 2H, 3D, 4E**). Neither the endogenous Nodal gradient nor endogenous endodermal cells are required to direct the sorting process. Our work defines an "AND" gate consisting of *sox32*-dependent endodermal specification and Nodal ligand reception that initiates the internalization process (**Fig. 3A**).

Nodal ligands specify both endodermal cell fate and endodermal sorting

Most of the focus on Nodal signaling during endoderm development has centered around its role in fate specification (Aoki, David, et al. 2002; Hagos and Dougan 2007; Dubrulle et al. 2015). Here we identified an additional role for Nodal as a signaling molecule that regulates endodermal sorting. Endodermal cells that either lack the ability to generate Nodal ligands or to receive Nodal ligands fail to undergo internalization when transplanted to the animal pole (**Fig. 2H, 4E**). Normally, both endoderm specification and Nodal ligand reception occur in the same location in the embryo near the margin, and activation of this "AND" gate (endodermal specification + Nodal ligand reception) could help specify when and where the internalization process occurs. The requirement for both Nodal ligands and endodermal specification could prevent non-endodermal cells that transiently receive Nodal ligands from internalizing. The autocrine nature of this circuit could help control the timing of internalization, which could be triggered when differentiation has proceeded sufficiently to drive this positive feedback loop. This positive feedback loop, in which cells that receive Nodal ligand input release more Nodal ligand, has previously been implicated in the large-scale self-organization of the Nodal field (Chan et al. 2009), and our work demonstrates an additional role for this feedback loop in coordinating endodermal cell sorting. This circuit could also enable the multicellular coordination of internalization. In chick embryos, single cell ingression can be amplified to induce more of the epiblast to undergo ingression (Voiculescu et al. 2014). Such community effect is Nodal-dependent and underlies the formation of primitive streak.

Nodal ligands are received through the Nodal receptor Acvr1ba and its co-receptor Tdgf1 (the zebrafish homolog of TDGF1/Cripto). The constitutively active Nodal receptor Acvr1ba* has frequently been used to investigate the Nodal signaling pathway (Schier and Shen 2000; Gritsman et al. 1999; Rachel M. Warga and Kane 2003). Surprisingly, we find that *acvr1ba** requires additional autocrine production and reception of Nodal ligands to support endodermal sorting (**Fig. 4**). Why might this be? One possibility is that internalization is only triggered above a certain threshold of Nodal signaling. For wild-type cells, this signaling threshold might only be achieved at the margin, where Nodal expression is highest, whereas cells expressing *acvr1ba**, in which Nodal signaling is activated beyond wild-type levels, can reach the thresholds needed for internalization even at positions far from the margin. However, in either case (wild-type or *acvr1ba**), these high signaling levels are achieved by a Nodal-induced Nodal expression positive feedback loop. In *acvr1ba**-induced endodermal cell, Smad2 activation levels are comparable with and without *ndr1/2* knockdown (**Fig. 2J-K**), suggesting *acvr1ba** can initiate Nodal signaling independent of Nodal ligands. In future experiments, this model could be tested by perturbing Smad function to varying degrees in the presence of *acvr1ba** and assessing the effects on ingression ability. An alternative explanation for the role of a Nodal autocrine circuit could be activation of *tdgf1*, which may have signaling roles independent of *acvr1ba*. This model would be consistent with previous literature showing that *acvr1ba** can only partially rescue *tdgf1* loss-of-function (Rachel M. Warga and Kane 2003). In future work, it will be interesting to further examine the differential signaling engaged by *acvr1ba** in the absence and presence of *tdgf1* to identify the *tdgf1*-specific effectors that could participate in endoderm migration.

Directional cues are not limited to Nodal ligands

We dissected the role of Nodal as a trigger for endodermal cell internalization. Through experiments with MZ *tdgf1* as a background for donor and host, we found that ectopic endodermal cells trigger sorting in an autocrine manner. By labeling the actin dynamics, we observed basal enrichment of actin-based protrusions, consistent with other reports suggesting that endodermal cells internalize through active migration(Giger and David 2017). Previous work in hydra also demonstrated the ability of individual endodermal cells to migrate towards the center of ectodermal aggregates, suggesting that invasion of endodermal cells into ectoderm may represent an ancient morphogenetic behavior (Takaku, Hariyama, and Fujisawa 2005).

But which spatial cues are these cells reading to migrate towards the interior of the embryo? We ruled out endogenous endodermal cells as an attractive positional cue because *acvr1ba**-expressing cells can ingress in the MZ *tdgf1* background, which lacks endogenous endodermal cells. Moreover, a functioning Nodal gradient does not exist in the MZ *tdgf1* host embryos, suggesting Nodal itself is not providing positional cues either. This latter point was further demonstrated in our experiments knocking down the endogenous Nodal gradient and flooding the embryo with uniform Nodal level, both of which failed to block ingression. The intersection of endodermal specification and Nodal ligand reception could unlock the ability of these cells to read other extracellular cues that are polarized from the outside to the inside of the embryo such as soluble ligands, ECM components, and mechanical cues (Piccolo 2013; Brunet et al. 2013). Apela (also known as Toddler and Elabela) functions as a motogen and enhances the movement of mesodermal and endodermal cells through Apelin receptor signaling, and Nodal is known to activate Apelin receptor expression (Pauli et al. 2014). However, we found that morpholino-directed knockdown of Apelin receptors a and b did not affect the ability of *acvr1ba**-induced cells to ingress into the interior of the embryo (**Fig. S10**), suggesting that Apela is unlikely to be the spatial cue. Alternatively, the cells could be responding to intrinsic polarity cues such as an oriented apical-basal polarity followed by apical constriction. Consistent with this idea, *Xenopus* bottle cells and *C.elegans* endodermal progenitor cells have apical-basal polarity and activate apical constriction to initiate gastrulation movements (Nance and Priess 2002). Clearly, additional work is needed to resolve this question.

Ingression functions as a pattern-refinement mechanism

This work aims to understand the molecular cues that initiate endodermal internalization and germ layer sorting. In addition to laying the foundation for coordinated cell movement at the primary site of endodermal cell internalization during normal development, single-cell ingression may also function as a backup plan to ensure that endodermal cells that are specified late or otherwise miss initial ingression can still find a path into the inner layer. Given that this sorting behavior is based on an autocrine circuit, endodermal cells can still ingress even if they are no longer adjacent to the margin, and this could increase the precision of the first step of endoderm morphogenesis.

From previous work on zebrafish morphogenesis, it is known that dorsal endodermal cells migrate highly asynchronously, which could lead to challenges in germ layer segregation (Keller et al. 2008). Cell sorting is thought to enable systems with initially noisy fate specification to generate robust final patterns. One extreme example is Dictyostelium, whose initial differentiation decision into prestalk or prespore cell is random, and differential migration is responsible for the final pattern (Dormann, Vasiev, and Weijer 2000). Similarly, during neural tube formation in zebrafish, heterogeneous sonic hedgehog responsivity is sharpened by neural progenitor cells sorting into discrete domains (Xiong et al. 2013). If migration were random, it would be expected to blur the boundaries between different germ layers for cells responding to a source of morphogen such as Nodal. In contrast, by linking directed migration to cell fate specification and signaling, this movement may instead improve the precision of the overall process. By establishing the necessary and sufficient triggers for endodermal sorting *in vivo*, our approach should be useful for continuing to define the logic of endodermal sorting during zebrafish gastrulation.

Materials and Methods

Zebrafish strains and embryos maintenance

Zebrafish maintenance was carried out under standard laboratory conditions in the zebrafish facility at Smith Cardiovascular Research Institute. Embryos were grown at 28-31°C in egg water and staged as described previously (Kimmel et al. 1995). The following wild-type (WT), mutant and transgenic lines were used: (WT) AB/TL; (mutant) *tdgf1*$^{tz57/+}$ (a generous gift from Lilianna Solnica-Krezel lab in Washington University in St. Louis); (transgenic) *Tg(sox17:GFP)*^{s870}, *Tg(sox17:DsRed)*^{s903}*Tg(h2afva:h2afva-mCherry)*^{tud7}*, Tg(ubb: GFP-Smad2)* ^{sfc16}*. Tg(sox17:GFP)*^{s870} and *Tg(sox17:DsRed)*^{s903} have been previously described (Chung and Stainier 2008; Mizoguchi et al. 2008). *Tg(h2afva:h2afva-mCherry)*^{tud7} has been previously described (Knopf et al. 2011). To construct *Tg(ubb:GFP-Smad2)*^{sfc16}, transgene plasmid mTol2-ubiq:GFP-Smad2 was created by separate PCR amplification of the ubiquitin promoter and GFP ORF and then cloned into pmTol2-ef1a:Venus-Smad2 (gift from Steve Harvey) cut with EcoRV and AgeI to remove the ef1a promoter and Venus ORF. *Tg(ubb:GFP-Smad2)*^{sfc16} was created by injecting 20 pg of the transgene plasmid DNA along with 100 pg of Tol2 transposase mRNA at the one cell stage. Injected embryos were then sorted by fluorescence on d0, raised to adulthood, and then screened for founders by outcrossing to wild-type.

Genotype analysis

Maternal zygotic tdgf1 *mutants.*

To create maternal zygotic *tdgf1* mutants, *tdgf1*$^{tz57/+}$ parents were in-crossed, and all embryos were injected with *tdgf1* mRNA so that homozygous embryos could survive. Genotyping was performed according to established protocols (Hashimoto et al. 2000 and Pogoda et al. 2000).

RNA expression constructs and morpholinos

Capped messenger RNA was synthesized using the mMESSAGE mMACHINE kit (Ambion). The following expression plasmids were used in this study: *acvr1ba** in pCS2 (pCS2-acvr1ba*-tBFP), full-length zebrafish *sox32* in pCS2 (pCS2-sox32; Chung and Stainier, 2008), *ndr1* and *ndr2* in pCS2 independently and GFP-UTRN in pCS2. The sox32 MO was designed to target the translation initiation site and was used at 2 ng (5′-CCTCCTCAGTGTTTATTTCGCTCAT-3′). *ndr1* MO (5'-ATGTCAAATCAAGGTAATAATCCAC-3′) and *ndr2* MO (5'-GCGACTCCCGAGCGTGTGCATGATG-3′) were used at 4ng. MOs targeting *aplnra* (5'-CGGTGTATTCCGGCGTTGGCTCCAT-3') and *aplnrb* (5'-CAGAGAAGTTGTTTGTCATGTGCTC-3') were injected at the one-cell stage at 1 ng or 0.5 ng, respectively.

mRNA, morpholino and dye injection

mRNA, morpholino and dye injections were performed with a micromanipulator connected to Picospritzer III. Drop size was regulated by the duration and pressure of the pulse. mRNA of appropriate concentration for different genes was injected into the yolk of the embryo at 1-cell stage. To obtain induced endodermal cells, 0.5pg *acvr1ba** mRNA or 100pg *sox32* mRNA were injected into the embryo. To study the effect of Nodal ligands on ingression, 4pg *ndr1* and *ndr2* mRNA were injected into the embryo. 200 pg GFP-UTRN was injected into the embryo to visualize actin dynamics. Morpholinos were briefly incubated at 65 °C to prevent precipitation and then injected into the yolk before the first cell division. 4ng *ndr1*, *ndr2* MO (Feldman and Stemple 2001; Karlen and Rebagliati 2001) or 2ng *sox32* MO (Sakaguchi, Kuroiwa, and Takeda 2001) or 1ng *aplnra* MO, 0.5ng *aplnrb* MO (Scott et al. 2007; Paskaradevan and Scott 2012; Pauli et al. 2014)was injected into the embryo to inhibit the translation of the corresponding genes. Dyes including Dextran-FITC or Dextran-tetra-methyl-rhodamin-dextran (TMR-dextran) or Dextran-Alexa Fluor 680 (LifeTechnologies) were injected at 1ng at the one-cell stage to label whole cells while 1 ng Histone H1 - Alexa Fluor 488 conjugate was injected into the embryo at 1-cell stage to label the nucleus.

Real-time quantitative PCR

For Nodal-activated conditions, wild-type embryos were injected at the one-cell stage with 2 pg *acvr1ba** mRNA or *mCherry* mRNA as a control. Expression of *sox17*, a known Nodal target gene, as well as *sox32*, were used to confirm Nodal activation. Expression of *cdh2* was measured under different Nodal-activated conditions. At shield stage, total RNA was extracted using the RNAqueous-Micro Kit, and 1 ng was used for reverse transcription with the SuperScript VILO cDNA Synthesis Kit (Invitrogen). The quantitative PCR reaction mixture contained 2 µl of 10-fold diluted cDNA, 12.5 µl SYBR green PCR master mix (Applied Biosystems), 714 nM of each primer, and nuclease-free water for a total volume of 25 µL in 48-well plates (Ilumina). Reactions were performed in the Eco Real-Time PCR System (Illumina, Inc.) as follows: initial activation at 95°C for 10 min followed by 40 cycles of 30 s at 95°C, 30 s at 60°C, and 30 s at 68°C. Once the PCR was completed, a melt-curve analysis was performed to determine reaction specificity. Samples were run in triplicate. The housekeeping gene *ef1a* was used as a reference. Refer to Tabel S1. List of Oligonucleotides for the primers used in this study.

Transplantation

Donor and host embryos were dechorionated with forceps under a dissection stereomicroscope and transferred into a glass plate with 0.3x Ringer's Buffer. 25~50 cells were taken from a dechorionated donor embryo(s) at sphere stage (4 hpf) and transplanted into the animal pole of a dechorionated host at the same stage using a bevelled borosilicate needle with a 35 µm inner diameter attached to a syringe system. In single donor transplantation experiments, the donor embryo was injected with mRNAs and/or morpholinos described in the main text and wild-type or MZ *tdgf1* embryos were used as hosts. In double donor transplantation experiments, the endoderm donor embryo was injected with 2pg *acvr1ba** mRNA, control ectoderm donor embryo was injected with 2ng *sox32* morpholino, and wild-type embryos were used as the host. Dextran dyes were used to differentiate donor versus host cells. H1 - Alexa Fluor 488 conjugate was used label the nucleus for single cell tracking. After transplantation, embryos were either immediately mounted for microscopy or maintained in 0.3x Ringer's Buffer at 28-31°C for further analysis.

Nodal inhibitor SB505124 treatment

For drug treatment, embryos from one dish were removed at the desired stage and split into glass dishes containing the drug in 5 ml embryo medium, at a density of 25 embryos/dish. For SB505124, the lowest dose that produced the sqt; cyc phenotype ranged from 30–50 μM, depending on the age of the drug (Hagos and Dougan 2007). Desired concentration is diluted from 10mM stock. For transplants, drug treatment is initiated after the transplantation is finished at 4hpf.

Time-lapse Confocal Microscopy

Dechorionated embryos, immediately after transplantation, were embedded in 1% low-melting agarose within glass-bottom Petri dishes, with animal pole mounted towards the glass bottom. For tracking, transplanted embryos were imaged with a 20x/0.75 NA Plan Fluor multi-immersion objective with water as the immersion media. For actin dynamics visualization, a 40x/1.15 NA water immersion objective was used. 10x/0.45 NA Plan Apo λ objective was used for imaging 24 hpf or 18-somite stage embryos. A high-speed widefield Nikon spinning disk confocal microscope was used for all imaging. This microscope is equipped with an Andor Borealis CSU-W1 unit, an Andor DU-888 EMCCD camera, and a stage-top incubator unit from OkoLab. Andor 4-line laser launch (100 mW at 405, 561, and 640 nm; 150 mW at 488 nm) was used for excitation. Micro-Manager Open Source Microscopy Software Version 2.0 Beta was used to control the microscope. Image stacks of 70-150 μm with 1-2 μm (1μm for timelapse and 2μm for end-point scanning) *z* stack were recorded in continuous mode, resulting in an image sampling rate of 2-4 min. Embryos were kept at 28.5°C throughout imaging.

Image Processing

Tracking with Gaussian Mixture Models (TGMM) software for automated large-scale segmentation and tracking of fluorescently labeled cell nuclei from the Keller Lab was adapted for single cell tracking of the transplanted cells (Amat et al. 2014). Timelapse datasets with Z-stacks were rendered into 3D tracks and filtered by track length. A sphere was used for modeling the zebrafish embryo, and Cartesian coordinates were transformed into spherical coordinates to determine the radial distance travelled by the transplanted cells.

Quantification and Statistical Analysis

Quantification of percentage of transplanted cell that localized to endodermal vs. non-endodermal domains was performed by analyzing images with Fiji. Z-stack images were converted to maximum intensity projections and thresholded by Renyi entropy. Particles were analyzed with Fiji and size of ROIs were measured. For image reslicing, Z-stack images were resliced to achieve 1 x 1 x 1 voxel size, then converted to maximum intensity projections to generate an XZ projection. Statistical data analysis was performed using Student's t-test in Matlab.

Acknowledgements

We thank Steve Harvey for plasmid (pmTol2-ef1a: Venus-Smad2), Lilianna Solnica-Krezel for providing the *tdgf1* zebrafish line, Philipp Keller for providing guidance on TGMM tracking software and Alba Diz-Muñoz for feedback on the manuscript. We are grateful to Jeremy Reiter, Wallace Marshall, Sophie Dumont and the Weiner group for fruitful discussions, and the zebrafish facility at CVRI and NIC at UCSF for assistance.

Footnotes

- **Competing interests**

  The authors declare no competing or financial interests.
- **Author Contributions**

  Conceptualization, Z.L. and O.W.; Methodology, Z.L. and S.W.; Formal Analysis, Z.L.; Writing – Original Draft, Z.L.; Writing – Review & Editing, O.W. and S.W.; Funding Acquisition, Z.L., S.W., and O.W.
- **Funding**

  This work was supported by a Genentech Predoctoral Fellowship (ZL), National Institutes of Health grants to SW (DK092312 and DK106358) and a National Institutes of Health grant (GM118167) and an American Heart Association Established Investigator Award to ODW.

References

Amat, Fernando, William Lemon, Daniel P. Mossing, Katie McDole, Yinan Wan, Kristin Branson, Eugene W. Myers, and Philipp J. Keller. 2014. “Fast, Accurate Reconstruction of Cell Lineages from Large-Scale Fluorescence Microscopy Data.” *Nature Methods* 11 (9): 951–58.

Aoki, Tazu O., Nicolas B. David, Gabriella Minchiotti, Laure Saint-Etienne, Thomas Dickmeis, Graziella M. Persico, Uwe Strähle, Philippe Mourrain, and Frédéric M. Rosa. 2002. “Molecular Integration of Casanova in the Nodal Signalling Pathway Controlling Endoderm Formation.” *Development* 129 (2): 275–86.

Aoki, Tazu O., Juliette Mathieu, Laure Saint-Etienne, Michael R. Rebagliati, Nadine Peyriéras, and Frédéric M. Rosa. 2002. “Regulation of Nodal Signalling and Mesendoderm Formation by TARAM-A, a TGFβ-Related Type I Receptor.” *Developmental Biology* 241 (2): 273–88.

Brunet, Thibaut, Adrien Bouclet, Padra Ahmadi, Démosthène Mitrossilis, Benjamin Driquez, Anne-Christine Brunet, Laurent Henry, et al. 2013. “Evolutionary Conservation of Early Mesoderm Specification by Mechanotransduction in Bilateria.” *Nature Communications* 4 (November).

Burkel, Brian M., George von Dassow, and William M. Bement. 2007. “Versatile Fluorescent Probes for Actin Filaments Based on the Actin-Binding Domain of Utrophin.” *Cell Motility and the Cytoskeleton* 64 (11): 822–32.

Carmany-Rampey, Amanda, and Alexander F. Schier. 2001. “Single-Cell Internalization during Zebrafish Gastrulation.” *Current Biology* 11 (16): 1261–65.

Chan, Tzu-Min, William Longabaugh, Hamid Bolouri, Hua-Ling Chen, Wen-Fang Tseng, Chung-Hao Chao, Te-Hsuan Jang, et al. 2009. “Developmental Gene Regulatory Networks in the Zebrafish Embryo.” *Biochimica et Biophysica Acta (BBA) - Gene Regulatory Mechanisms*, System Biology – Genetic Networks, 1789 (4): 279–98.

Chen, Yu, and Alexander F. Schier. 2001. “The Zebrafish Nodal Signal Squint Functions as a Morphogen.” *Nature* 411 (6837): 607–10.

Chung, Won-Suk, and Didier Y. R. Stainier. 2008. “Intra-Endodermal Interactions Are Required for Pancreatic β Cell Induction.” *Developmental Cell* 14 (4): 582–93.

Concha, M. L., and R. J. Adams. 1998. “Oriented Cell Divisions and Cellular Morphogenesis in the Zebrafish Gastrula and Neurula: A Time-Lapse Analysis.” *Development* 125 (6): 983–94.

D’Amico, L. A., and M. S. Cooper. 1997. “Spatially Distinct Domains of Cell Behavior in the Zebrafish Organizer Region.” *Biochemistry and Cell Biology = Biochimie Et Biologie Cellulaire* 75 (5): 563–77.

David, Nicolas B., and Frédéric M. Rosa. 2001. “Cell Autonomous Commitment to an Endodermal Fate and Behaviour by Activation of Nodal Signalling.” *Development* 128 (20): 3937–47.

Dickmeis, Thomas, Philippe Mourrain, Laure Saint-Etienne, Nadine Fischer, Pia Aanstad, Matthew Clark, Uwe Strähle, and Frédéric Rosa. 2001. “A Crucial Component of the Endoderm Formation Pathway, CASANOVA, Is Encoded by a Novel Sox-Related Gene.” *Genes & Development* 15 (12): 1487–92.

Dormann, Dirk, Bakhtier Vasiev, and Cornelis J. Weijer. 2000. “The Control of Chemotactic Cell Movement during Dictyostelium Morphogenesis.” *Philosophical Transactions of the Royal Society of London. Series B: Biological Sciences* 355 (1399): 983–91.

Dougan, Scott T., Rachel M. Warga, Donald A. Kane, Alexander F. Schier, and William S. Talbot. 2003. “The Role of the Zebrafish Nodal-Related Genes Squint and Cyclops in Patterning of Mesendoderm.” *Development* 130 (9): 1837–51.

Dubrulle, Julien, Benjamin M. Jordan, Laila Akhmetova, Jeffrey A. Farrell, Seok-Hyung Kim, Lilianna Solnica-Krezel, and Alexander F. Schier. 2015. “Response to Nodal Morphogen Gradient Is Determined by the Kinetics of Target Gene Induction.” *eLife* 4 (April): e05042.

Erter, Caroline E, Lilianna Solnica-Krezel, and Christopher V. E Wright. 1998. “Zebrafish Nodal-Related 2Encodes an Early Mesendodermal Inducer Signaling from the Extraembryonic Yolk

Syncytial Layer.” *Developmental Biology* 204 (2): 361–72.

Feldman, Benjamin, Michael A. Gates, Elizabeth S. Egan, Scott T. Dougan, Gabriela Rennebeck, Howard I. Sirotkin, Alexander F. Schier, and William S. Talbot. 1998. “Zebrafish Organizer Development and Germ-Layer Formation Require Nodal-Related Signals.” *Nature* 395 (6698): 181–85.

Feldman, Benjamin, and Derek L. Stemple. 2001. “Morpholino Phenocopies of Sqt, Oep, and Ntl Mutations.” *Genesis* 30 (3): 175–77.

Giger, Florence A., and Nicolas B. David. 2017. “Endodermal Germ-Layer Formation through Active Actin-Driven Migration Triggered by N-Cadherin.” *Proceedings of the National Academy of Sciences* 114 (38): 10143–48.

Gritsman, Kira, Jiaojiao Zhang, Simon Cheng, Elizabeth Heckscher, William S. Talbot, and Alexander F. Schier. 1999. “The EGF-CFC Protein One-Eyed Pinhead Is Essential for Nodal Signaling.” *Cell* 97 (1): 121–32.

Hagos, Engda G, and Scott T Dougan. 2007. “Time-Dependent Patterning of the Mesoderm and Endoderm by Nodal Signals in Zebrafish.” *BMC Developmental Biology* 7 (1): 22.

Hashimoto, Hisashi, Motoyuki Itoh, Yojiro Yamanaka, Susumu Yamashita, Takashi Shimizu, Lilianna Solnica-Krezel, Masahiko Hibi, and Toshio Hirano. 2000. “Zebrafish Dkk1 Functions in Forebrain Specification and Axial Mesendoderm Formation.” *Developmental Biology* 217 (1): 138–52.

Ho, R. K. 1992. “Cell Movements and Cell Fate during Zebrafish Gastrulation.” *Development (Cambridge, England). Supplement*, 65–73.

Jia, Shunji, Zhen Ren, Xiang Li, Ying Zheng, and Anming Meng. 2008. “smad2 and smad3 Are Required for Mesendoderm Induction by Transforming Growth Factor-β/Nodal Signals in Zebrafish.” *Journal of Biological Chemistry* 283 (4): 2418–26.

Jing, Xiao-hong, Sheng-mei Zhou, Wei-qing Wang, and Yu Chen. 2006. “Mechanisms

Underlying Long- and Short-Range Nodal Signaling in Zebrafish." *Mechanisms of Development* 123 (5): 388–94.

Karlen, Sarah, and Michael Rebagliati. 2001. "A Morpholino Phenocopy of the Cyclops Mutation." *Genesis* 30 (3): 126–28.

Keller, Philipp J., Annette D. Schmidt, Joachim Wittbrodt, and Ernst H. K. Stelzer. 2008. "Reconstruction of Zebrafish Early Embryonic Development by Scanned Light Sheet Microscopy." *Science* 322 (5904): 1065–69.

Kikuchi, Yutaka, Antoine Agathon, Jonathan Alexander, Christine Thisse, Steven Waldron, Deborah Yelon, Bernard Thisse, and Didier Y. R. Stainier. 2001. "Casanova Encodes a Novel Sox-Related Protein Necessary and Sufficient for Early Endoderm Formation in Zebrafish." *Genes & Development* 15 (12): 1493–1505.

Kimmel, Charles B., William W. Ballard, Seth R. Kimmel, Bonnie Ullmann, and Thomas F. Schilling. 1995. "Stages of Embryonic Development of the Zebrafish." *Developmental Dynamics* 203 (3): 253–310.

Kimmel, Charles B., and Rachel M. Warga. 1987. "Cell Lineages Generating Axial Muscle in the Zebrafish Embryo." *Nature* 327 (6119): 234.

Knopf, Franziska, Christina Hammond, Avinash Chekuru, Thomas Kurth, Stefan Hans, Christopher W. Weber, Gina Mahatma, et al. 2011. "Bone Regenerates via Dedifferentiation of Osteoblasts in the Zebrafish Fin." *Developmental Cell* 20 (5): 713–24.

Krens, S. F. Gabriel, Jim H. Veldhuis, Vanessa Barone, Daniel Čapek, Jean-Léon Maître, G. Wayne Brodland, and Carl-Philipp Heisenberg. 2017. "Interstitial Fluid Osmolarity Modulates the Action of Differential Tissue Surface Tension in Progenitor Cell Segregation during Gastrulation." *Development* 144 (10): 1798–1806.

Krieg, M., Y. Arboleda-Estudillo, P.-H. Puech, J. Käfer, F. Graner, D. J. Müller, and C.-P. Heisenberg. 2008. "Tensile Forces Govern Germ-Layer Organization in Zebrafish." *Nature Cell Biology* 10 (4): 429–36.

Lewis, Julian. 1985. “Cells into Organs (the Forces That Shape the Embryo): By John Philip Trinkaus, Prentice-Hall Inc, 1984. £37.90 (xxvi + 543 Pages) ISBN 0 13 121632 5.” *Trends in Neurosciences* 8 (January): 422.

Maître, Jean-Léon, Hélène Berthoumieux, Simon Frederik Gabriel Krens, Guillaume Salbreux, Frank Jülicher, Ewa Paluch, and Carl-Philipp Heisenberg. 2012. “Adhesion Functions in Cell Sorting by Mechanically Coupling the Cortices of Adhering Cells.” *Science* 338 (6104): 253–56.

Mizoguchi, Takamasa, Heather Verkade, Joan K. Heath, Atsushi Kuroiwa, and Yutaka Kikuchi. 2008. “Sdf1/Cxcr4 Signaling Controls the Dorsal Migration of Endodermal Cells during Zebrafish Gastrulation.” *Development* 135 (15): 2521–29.

Montero, Juan-Antonio, Lara Carvalho, Michaela Wilsch-Bräuninger, Beate Kilian, Chigdem Mustafa, and Carl-Philipp Heisenberg. 2005. “Shield Formation at the Onset of Zebrafish Gastrulation.” *Development* 132 (6): 1187–98.

Nair, Sreelaja, and Thomas F. Schilling. 2008. “Chemokine Signaling Controls Endodermal Migration During Zebrafish Gastrulation.” *Science* 322 (5898): 89–92.

Nance, Jeremy, and James R. Priess. 2002. “Cell Polarity and Gastrulation in *C. Elegans*.” *Development* 129 (2): 387–97.

Paskaradevan, Sivani, and Ian C. Scott. 2012. “The Aplnr GPCR Regulates Myocardial Progenitor Development via a Novel Cell-Non-Autonomous, Gαi/o Protein-Independent Pathway.” *Biology Open* 1 (3): 275–85.

Pauli, Andrea, Megan L. Norris, Eivind Valen, Guo-Liang Chew, James A. Gagnon, Steven Zimmerman, Andrew Mitchell, et al. 2014. “Toddler: An Embryonic Signal That Promotes Cell Movement via Apelin Receptors.” *Science* 343 (6172): 1248636.

Piccolo, Stefano. 2013. “Developmental Biology: Mechanics in the Embryo.” *Nature* 504 (7479): 223–25.

Pogoda, Hans-Martin, Lilianna Solnica-Krezel, Wolfgang Driever, and Dirk Meyer. 2000. “The Zebrafish Forkhead Transcription Factor FoxH1/Fast1 Is a Modulator of Nodal Signaling Required for Organizer Formation.” *Current Biology* 10 (17): 1041–49.

Renucci, A., V. Lemarchandel, and F. Rosa. 1996. “An Activated Form of Type I Serine/threonine Kinase Receptor TARAM-A Reveals a Specific Signalling Pathway Involved in Fish Head Organiser Formation.” *Development* 122 (12): 3735–43.

Sakaguchi, Takuya, Atsushi Kuroiwa, and Hiroyuki Takeda. 2001. “A Novel Sox Gene, 226D7, Acts Downstream of Nodal Signaling to Specify Endoderm Precursors in Zebrafish.” *Mechanisms of Development* 107 (1): 25–38.

Schier, Alexander F., and Michael M. Shen. 2000. “Nodal Signalling in Vertebrate Development.” *Nature* 403 (6768): 385–89.

Scott, Ian C., Bernard Masri, Leonard A. D’Amico, Suk-Won Jin, Benno Jungblut, Ann M. Wehman, Herwig Baier, Yves Audigier, and Didier Y. R. Stainier. 2007. “The G Protein-Coupled Receptor Agtrl1b Regulates Early Development of Myocardial Progenitors.” *Developmental Cell* 12 (3): 403–13.

Shivdasani, Ramesh A. 2002. “Molecular Regulation of Vertebrate Early Endoderm Development.” *Developmental Biology* 249 (2): 191–203.

Steinberg, Malcolm S. 1962. “On the Mechanism of Tissue Reconstruction by Dissociated Cells, I. Population Kinetics, Differential Adhessiveness, and the Absence of Directed Migration*.” *Proceedings of the National Academy of Sciences of the United States of America* 48 (9): 1577–82.

Stern, Claudio D. 2004. *Gastrulation: From Cells To Embryo*. Cold Spring Harbor Laboratory Press.

Takaku, Yasuharu, Takahiko Hariyama, and Toshitaka Fujisawa. 2005. “Motility of Endodermal Epithelial Cells Plays a Major Role in Reorganizing the Two Epithelial Layers in Hydra.” *Mechanisms of Development* 122 (1): 109–22.

Voiculescu, Octavian, Lawrence Bodenstein, I.-Jun Lau, and Claudio D. Stern. 2014. “Local Cell Interactions and Self-Amplifying Individual Cell Ingression Drive Amniote Gastrulation.” *eLife* 3 (May): e01817.

Warga, Rachel M., and Donald A. Kane. 2003. “One-Eyed Pinhead Regulates Cell Motility Independent of Squint/Cyclops Signaling.” *Developmental Biology* 261 (2): 391–411.

Warga, R. M., and C. B. Kimmel. 1990. “Cell Movements during Epiboly and Gastrulation in Zebrafish.” *Development* 108 (4): 569–80.

Weng, Wei, and Derek L. Stemple. 2003. “Nodal Signaling and Vertebrate Germ Layer Formation.” *Birth Defects Research Part C: Embryo Today: Reviews* 69 (4): 325–32.

Wolpert, L. 1992. “Gastrulation and the Evolution of Development.” *Development (Cambridge, England). Supplement*, 7–13.

Woo, Stephanie, Michael P. Housley, Orion D. Weiner, and Didier Y. R. Stainier. 2012. “Nodal Signaling Regulates Endodermal Cell Motility and Actin Dynamics via Rac1 and Prex1.” *The Journal of Cell Biology* 198 (5): 941–52.

Xiong, Fengzhu, Andrea R. Tentner, Peng Huang, Arnaud Gelas, Kishore R. Mosaliganti, Lydie Souhait, Nicolas Rannou, et al. 2013. “Specified Neural Progenitors Sort to Form Sharp Domains after Noisy Shh Signaling.” *Cell* 153 (3): 550–61.

Figures

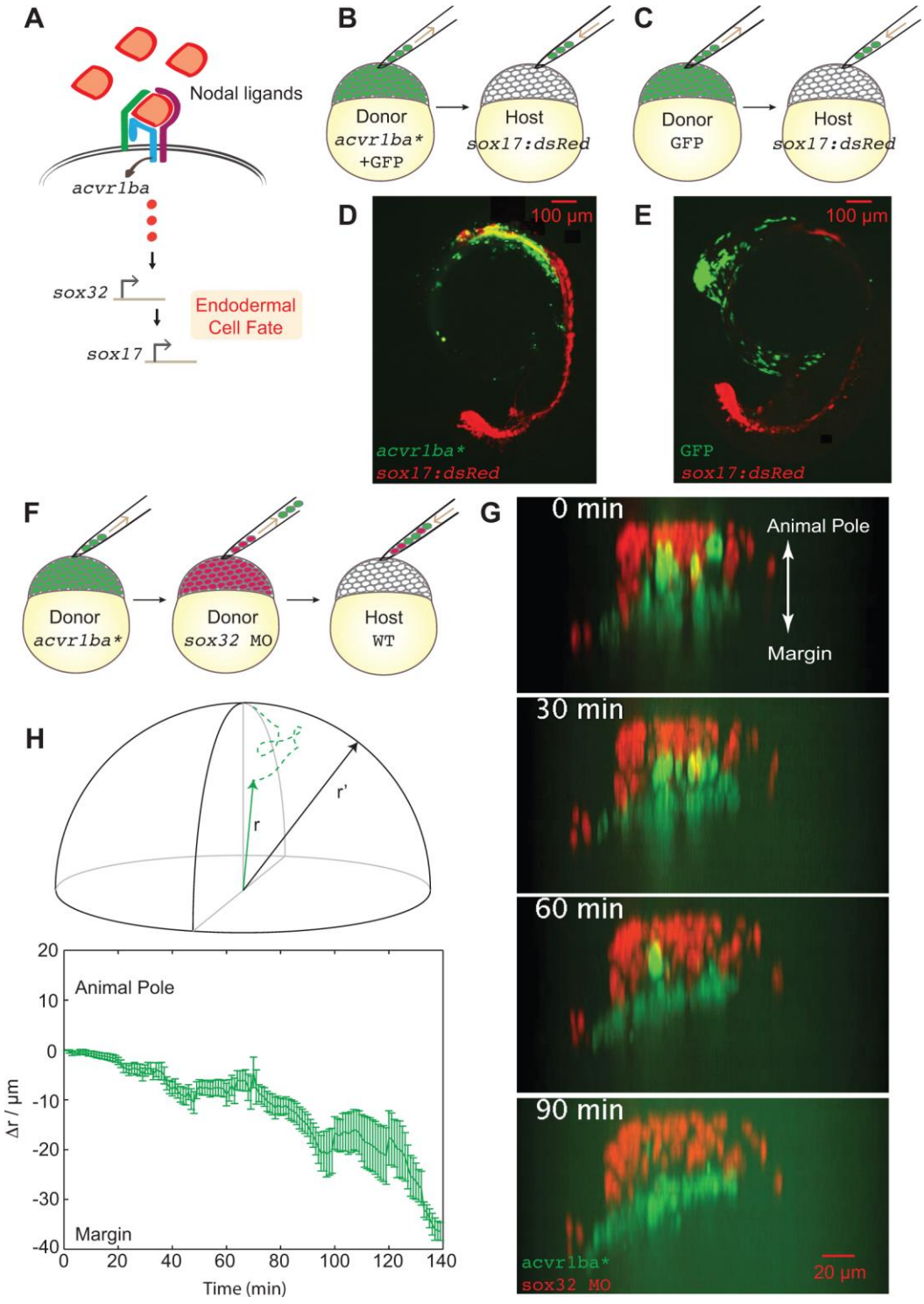

Figure 1:

Constitutively active Nodal receptor (*acvr1ba)-induced ectopic endodermal cells sort into the inner layer of the embryo by ingression.**

(A) Schematic diagram depicting Nodal signaling and specification of endodermal cell fate. Nodal ligands activate the *acvr1ba* receptor and signal to *sox32*, a transcription factor controlling endodermal specification.

(B-E) Schematic diagrams of ectopic endoderm transplant assay (B, C) and representative results (D, E). *acvr1ba**-expressing or control cells were transplanted to the animal pole of *Tg(sox17:dsRed)* host embryos. At 21-somite stage, transplanted *acvr1ba**-expressing cells localized to endoderm-derived tissue, primarily the pharynx, (D) while control transplanted cells localized to non-endodermal tissue, particularly the head (E).

(F) Schematic diagram of the double donor transplant assay. Donor endodermal cells expressing *acvr1ba** (green) were transplanted together with non-endodermal donor cells injected with *sox32* MO (red) to the animal pole of a single wild-type host.

(G) Still images from a time-lapse movie of a WT host containing both *acvr1ba**-expressing (green) and *sox32* MO-containing (red) donor cells. Time lapse microscopy began immediately after transplantation (0 min). Over time, *sox32* MO donor cells remain in the outer layer of the embryo, while *acvr1ba**-expressing donor cells migrate into the inner layer of the embryo. Data was resliced and projected onto the XZ plane, with the animal pole towards the top and the margin towards the bottom.

(H) Single-cell tracking analysis of ingression. Top panel: Cartesian coordinates for transplanted cells were transformed into spherical coordinates. Dashed lines represent cell trajectories. The radial distance, r, was measured as the distance from each cell's position at the end of the time lapse movie to the center of the embryo (solid lines). r' was measured as the distance to the host surface for normalization. Bottom panel: Average relative distance with standard error of *acvr1ba**-expressing cells plotted against time. Relative distance for each time point was calculated by measuring the radial distance of *acvr1ba**-expressing cells to the center of the embryo, subtracted by the distance of host cell expanding during gastrulation.

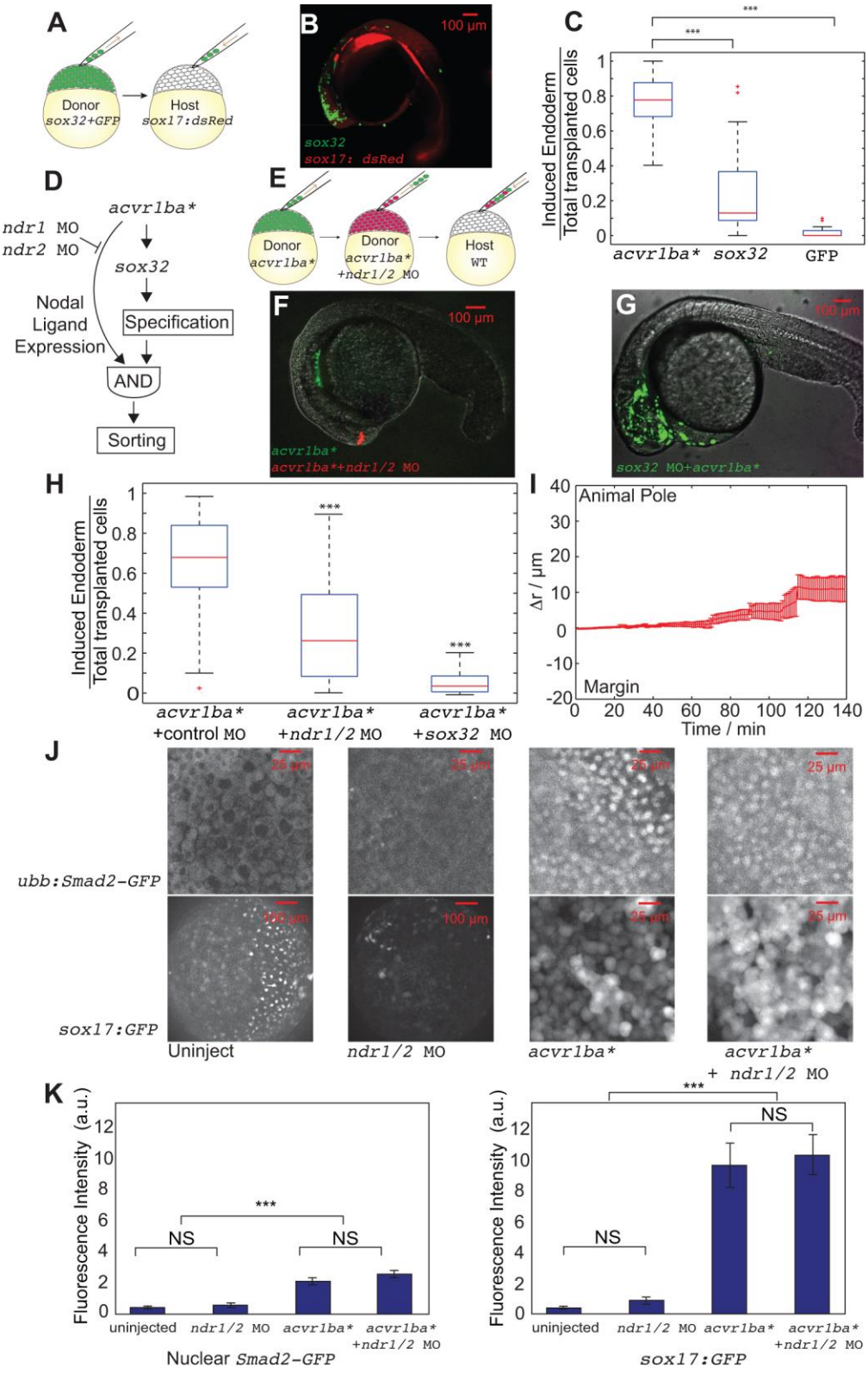

Figure 2:

Nodal ligand expression is necessary to trigger the sorting of ectopic *acvr1ba-induced endodermal cells.**

(A-B) Schematic diagrams depicting *sox32*-induced ectopic endoderm transplant assay (A) and representative result (B). *sox32*-overexpressing cells were transplanted to the animal pole of wild-type host embryos. At 21-somite stage, transplanted *sox32*-overexpressing cells primarily localized to non-endodermal tissues, primarily in the head and skin.

(C) Boxplot quantification of endoderm contribution of transplanted cells at 20 hpf, assessed by co-localization with *Tg(sox17:dsRed)* expression. On each box, the central mark indicates the median, and the bottom and top edges of the box indicate the 25th and 75th percentiles, respectively. The whiskers extend to the most extreme data points not considered outliers, and the outliers are plotted individually using the '+' symbol. Compared to *acvr1ba**-expressing cells, fewer cells overexpressing *sox32* contributed to endodermal tissues. Data is shown as mean ± SEM of 3 independent transplantation experiments with 26 embryos per condition. Student's t-test was performed. * $p<0.05$, ** $p<0.01$, *** $p<0.001$.

(D) Schematic diagram depicting a potential AND gate for endoderm sorting. Constitutively activate *acvr1ba** upregulates both *sox32* as well as Nodal ligand expression. Only with both inputs do cells successfully sort to the inner layer of the embryo.

(E) Schematic diagram of the cell transplantation assay to test the necessity of Nodal ligand expression for cell sorting. Donor cells containing *ndr1* and *ndr2* MOs plus *acvr1ba** mRNA (red) were transplanted together with cells overexpressing *acvr1ba** only (green) into the animal pole of a wild-type host embryo.

(F) Representative images showing distribution of transplanted cells at 21-somite stage. Cells expressing *acvr1ba** only (green) localize to endoderm-derived tissue, primarily the pharynx. Cells containing *acvr1ba** along with *ndr1* MO and *ndr2* MO (red) localize to non-endodermal tissue, primarily in the head. Lateral view, anterior to the bottom-left.

(G) Representative images showing distribution of transplanted cells at 21-somite stage. Cells expressing *acvr1ba** along with *sox32* MO (green) localize to ectoderm-derived tissue, primarily the head. Lateral view, anterior to the bottom-left.

(H) Boxplot quantification of endoderm contribution of transplanted cells at 20 hpf. *ndr1* and *ndr2* knockdown as well as *sox32* knockdown reduced the ability of *acvr1ba**-expressing cells to contribute to endodermal tissue. Data is shown as mean ± SEM of 3 independent transplantation experiments with 22 embryos per condition. Student's t-test was performed. * $p<0.05$, ** $p<0.01$, *** $p<0.001$.

(I) Single-cell tracking analysis of ingression of *acvr1ba**-expressing cells with *ndr1* MO and *ndr2* MO. Average relative distance with standard error plotted against time. Relative distance was calculated as in Fig. 1H.

(J) Nodal signaling levels assessed by *Tg(ubb:Smad2-GFP)* and *Tg(sox17:GFP)*. Top panel: Smad2-GFP showed no nuclear localization in cells at the animal poles (AP) of uninjected embryos and *ndr*1/*ndr2* morphants. Smad2-GFP showed comparable levels of nuclear localization in *acvr1ba**-injected embryos and *acvr1ba** with and *ndr1* and *ndr2* MOs-injected embryos. Bottom Panel: Sox17:GFP labels wild-type endodermal cells in the uninjected control embryo but few GFP-positive cells are present in the *ndr1*/*ndr2* morphants. Animal Pole View. Sox17:GFP shows elevated level of expression in both *acvr1ba** injected embryos and *acvr1ba** with and *ndr1* and *ndr2* MOs injected embryos. Lateral view. Margin depicted by dash line.

(K) Quantification of Nodal signaling level. Nuclear Smad2-GFP and Sox17:GFP fluorescence levels are quantified. Data is shown as mean ± SEM of 3 independent embryos.

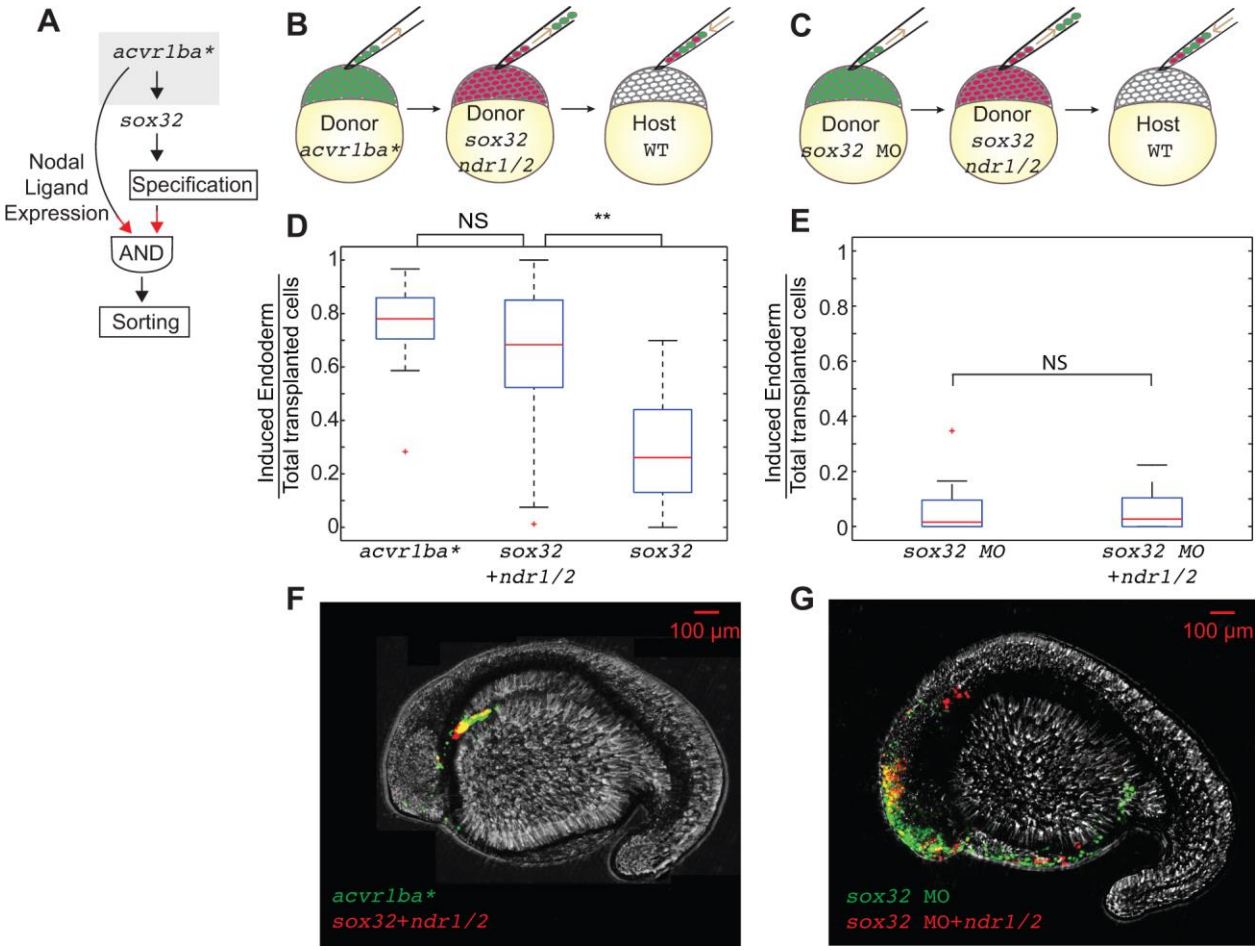

Figure 3:

The combination of Nodal ligand expression and endodermal fate is sufficient to trigger ectopic endodermal cell sorting.

(A) Schematic diagram depicting putative AND gate for endoderm sorting. Red arrows demonstrate the experimental perturbation to test the sufficiency of Nodal ligands to induce ingression.

(B-C) Schematic diagrams of double transplantation assay to test the sufficiency of the AND gate depicted in (A) for endodermal sorting. Cells overexpressing *acvr1ba** (green) were transplanted together with cells overexpressing *sox32*, *ndr1*, and *ndr2* (red) into the animal pole of a wild-type host embryo (B). Cells containing *sox32* MO only were transplanted together with cells containing *sox32* MO as well as *ndr1* and *ndr2* mRNAs were transplanted into the animal pole of a wild-type host embryo (C).

(D) Boxplot quantification of endoderm contribution at 20 hpf of transplanted cells depicted in (B). Cells overexpressing *sox32*, *ndr1*, and *ndr2* contributed to endoderm at a similar rate compared to cells overexpressing *acvr1ba**. Data is shown as mean ± SEM of 3 independent transplantation experiments with 18 embryos per condition. Student's t-test was performed. * $p<0.05$, ** $p<0.01$, *** $p<0.001$.

(E) Boxplot quantification of endoderm contribution at 20 hpf of transplanted cells depicted in (C). Neither cells containing *sox32* MO nor cells containing *sox32* MO and overexpressing *ndr1* and *ndr2* contributed to endodermal tissue. In addition, cells expressing *acvr1ba** and *sox32* MO did not contribute to endodermal tissue. Data is shown as mean ± SEM of 2 independent transplantation experiments with 14 embryos per condition. Student's t-test was performed. * $p<0.05$, ** $p<0.01$, *** $p<0.001$.

(F) Representative image showing distribution of transplanted cells depicted in (B) at 18-somite stage. *acvr1ba**-expressing cells localized to the endoderm-derived tissue, primarily the pharynx (green). Cells overexpressing *sox32*, *ndr1*, and *ndr2* also localize to endoderm-derived tissue, primarily the pharynx (red). Lateral view, anterior to the left.

(G) Representative image showing distribution of transplanted cells depicted in (E) at 18-somite stage. Cells expressing *sox32* and Nodal ligands (*ndr1*, *ndr1*) localize to endodermal tissues similar to cells expressing *acvr1ba**. In contrast, *sox32* MO-injected cells (green) and cells injected with *sox32* MO and *ndr1* and *ndr2* mRNAs (red) localized to non-endodermal tissue, primarily in the head and skin.

(H) Representative image showing distribution of transplanted cells injected with *sox32* MO and *acvr1ba** at 21-somite stage. Transplanted cells (green) mainly localized to non-endodermal tissue. Lateral view, anterior to the left.

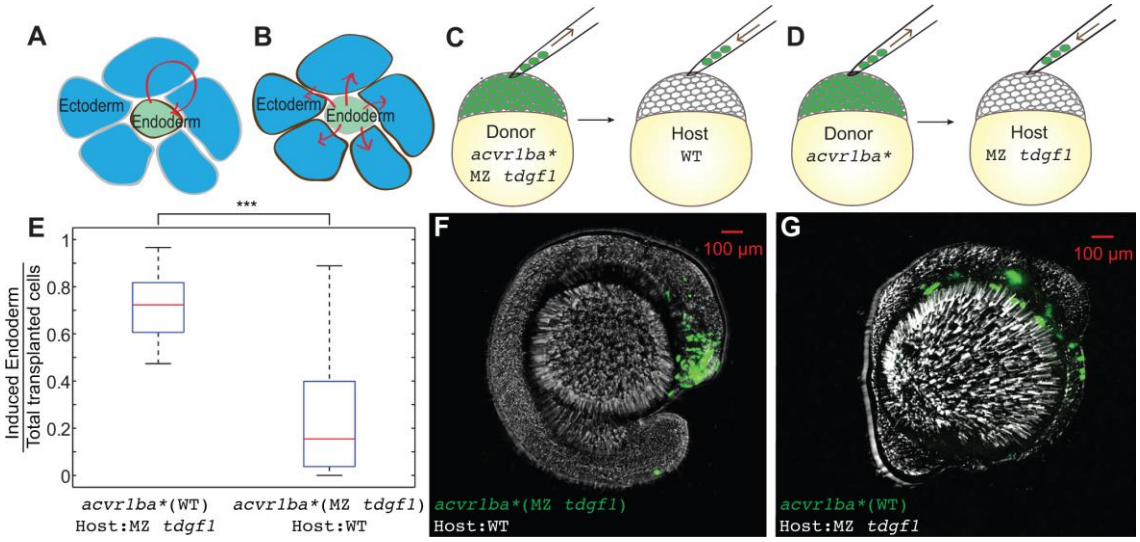

Figure 4:

Nodal ligand reception acts cell autonomously to support sorting.

(A-B) Schematic diagrams depicting autonomous (A) versus non-autonomous (B) Nodal ligand reception (red arrows).

(C) Schematic diagram depicting single donor transplant assay to test cell autonomous Nodal signal reception. *acvr1ba**-expressing cells from MZ *tdgf1* donor embryos were transplanted to the animal pole of a wild-type host embryo.

(D) Schematic diagram depicting single donor transplant assay to test cell non-autonomous Nodal signal reception. *acvr1ba**-expressing cells from wild-type donor embryos were transplanted to the animal pole of a MZ *tdgf1* host embryo.

(E) Boxplot quantification of endoderm contribution at 18-somite stage for all transplanted cells. Wild-type donor cells expressing *acvr1ba** contributed to endodermal tissues while *acvr1ba**-expressing cells from MZ *tdgf1* embryos did not. Data is shown as mean ± SEM of 2 independent transplantation experiments, with 14 embryos per condition. Student's t-test was performed. * $p<0.05$, ** $p<0.01$, *** $p<0.001$.

(F) Representative image showing distribution of MZ *tdgf1* cells expressing *acvr1ba** in a wild-type host. Donor cells (green) localized to ectoderm-derived tissue, primarily the head. Lateral view, anterior to the right.

(G) Representative image showing distribution of wild-type cells expressing *acvr1ba** in a MZ *tdgf1* host. Donor cells (green) localized to endoderm-derived tissue. Lateral view, anterior to the right.

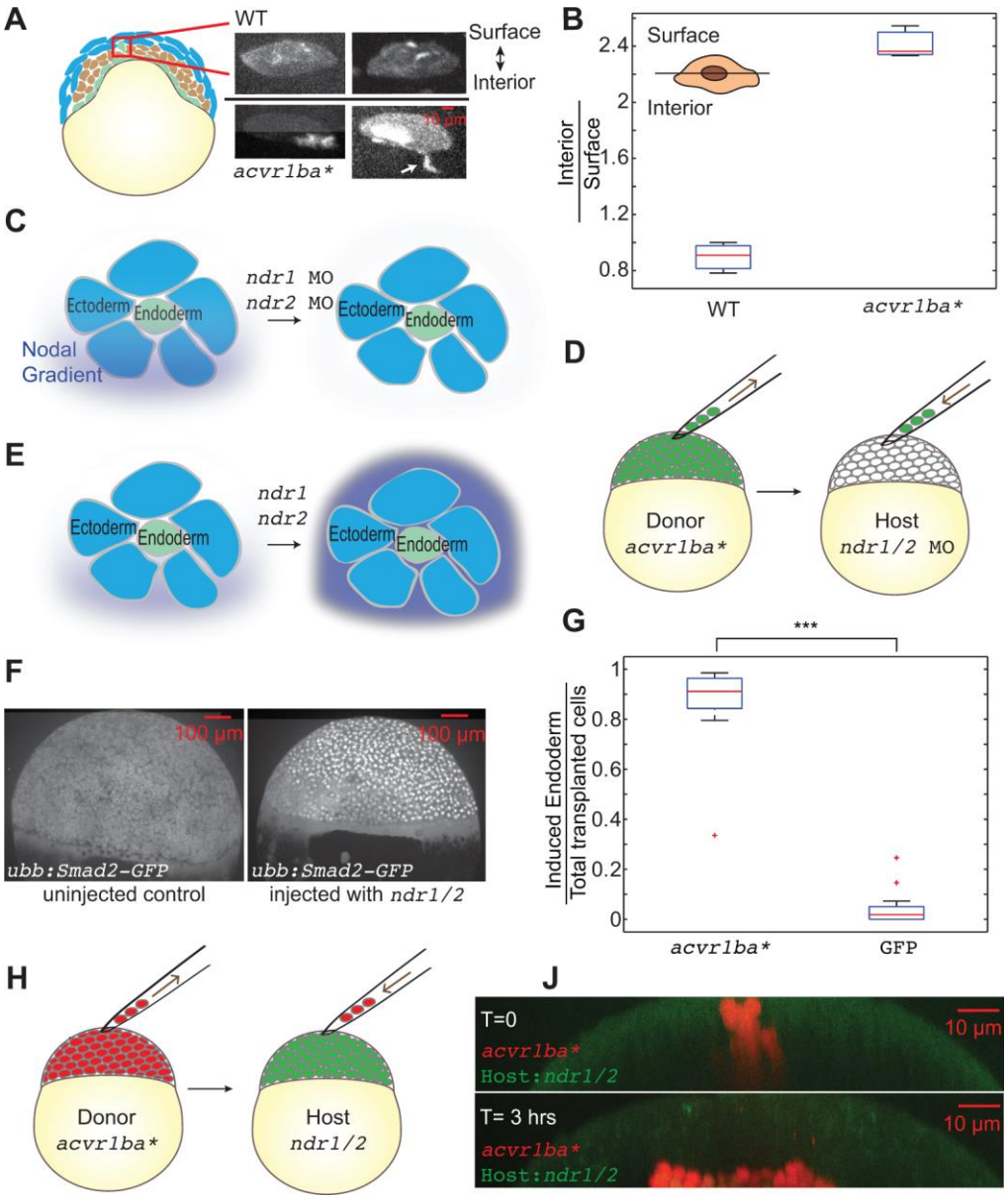

Figure 5:

Nodal ligands initiate but do not guide the ingression of endodermal cells.

(A) Actin localization in ectopic endodermal cells. Blue, ectoderm; brown, mesoderm; green, endoderm Donor embryos were injected with GFP-UTRN mRNA to label actin filaments. Cells overexpressing *acvr1ba** or control cells expressing GFP-UTRN only were transplanted to the animal poles of wild-type host embryos. Actin was enriched on the interior side of *acvr1ba**-expressing cells while control cells exhibited uniform actin distribution. Data is resliced and projected to the XZ plane, with the surface of the embryo towards the top and the interior towards the bottom. Arrow shows interior-facing protrusion.

(B) Boxplot of the ratio of interior to surface accumulation of actin. *acvr1ba**-expressing cells exhibited significant interior enrichment of actin compared to control cells. Data is shown as mean ± SEM of 3 independent transplantation experiments, with 58 cells per condition. Student's t-test was performed. * $p<0.05$, ** $p<0.01$, *** $p<0.001$.

(C-E) Determining whether the endogenous Nodal gradient functions as a directional cue for endoderm ingression through knockdown of endogenous Nodal ligands. (C) *ndr1* and *ndr2* MOs were injected into host embryos to remove the endogenous Nodal gradient. (D) Cells expressing *acvr1ba** were transplanted to the animal pole of a Nodal-depleted host. (E) Boxplot quantification of endoderm contribution at 20 hpf for all transplanted cells. Cells overexpressing *acvr1ba** still contributed to endodermal tissues even in the absence of an endogenous Nodal gradient. Data is shown as mean ± SEM of 2 independent transplantation experiments, with 15 embryos per condition. Student's t-test was performed. * $p<0.05$, ** $p<0.01$, *** $p<0.001$.

(F-I) Saturating the endogenous Nodal gradient to test whether it acts as a directional cue. (G) *ndr1* and *ndr2* mRNAs were injected into host embryos to produce uniform Nodal expression. (H) *Tg(ubb:Smad2-GFP)* shows uniform nuclear translocation in a *ndr1* and *ndr2* injected embryo, suggesting uniform Nodal signaling. (I) Cells expressing *acvr1ba** were transplanted to the animal pole of a Nodal-saturated host. (J) Representative image showing positions of *acvr1ba** cells (red) immediately and 3 hours after transplantation in a Nodal-saturated host.

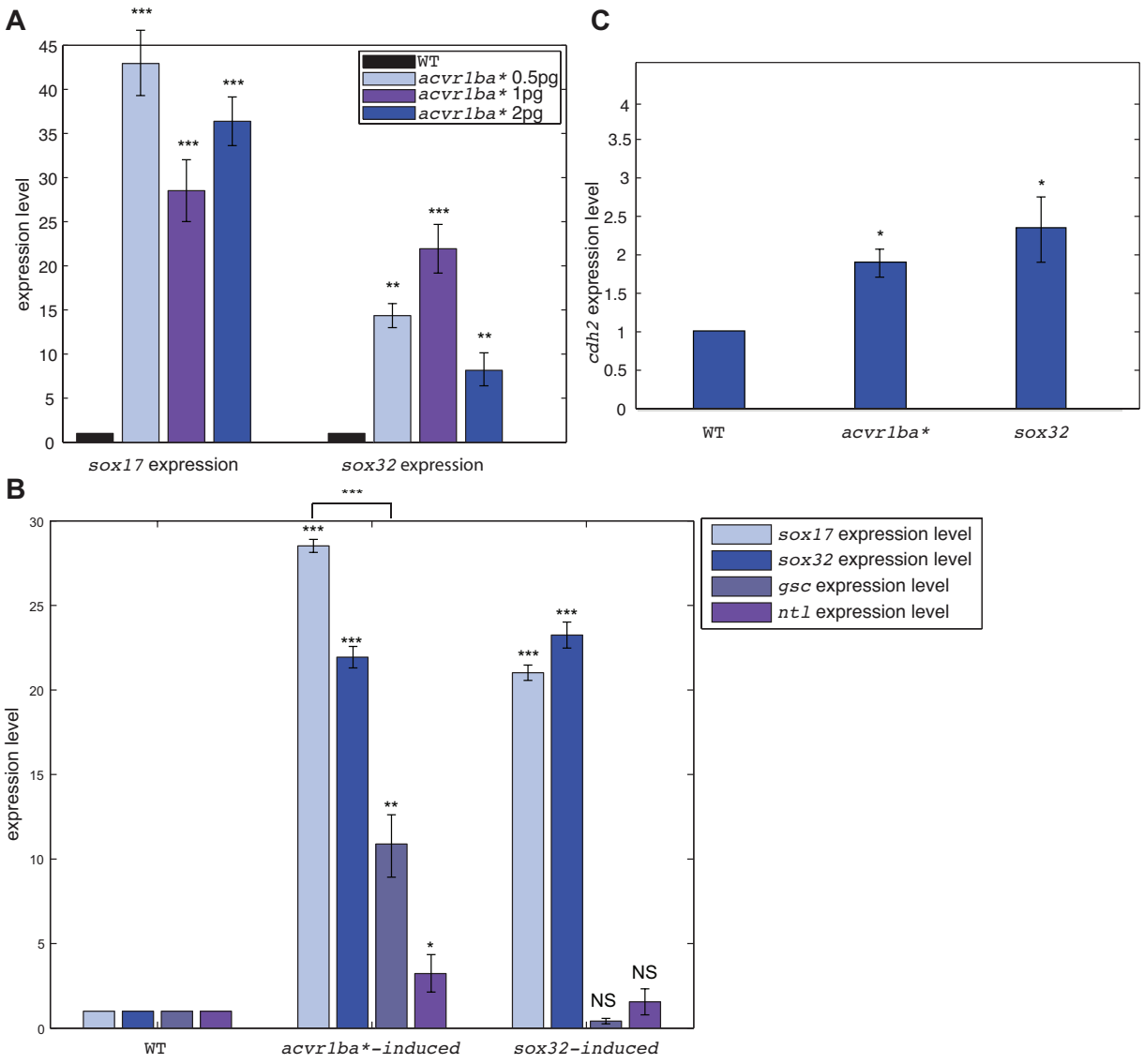

Figure S1: ***acvr1ba**** **induces expression of *sox17* and *sox32*. Related to Figure 1.**

(A) Expression of *sox17* and *sox32* endodermal markers was measured by real-time quantitative PCR. Constitutive activation of the Nodal pathway by expression of *acvr1ba** upregulated *sox17* and *sox32* expression (normalized to uninjected controls). **p<0.01, ***p<0.001.

(B) Expression of *sox17*, *sox32*, *gsc* and *ntl* was measured by real-time quantitative PCR in *acvr1ba**-expressing cells and *sox32*-expressing cells in wildtype background. Both acvrb1a* and sox32 more potently induce endodermal markers (*sox17* and *sox32*) than mesodermal markers (*gsc* and *ntl*). *p<0.05, **p<0.01, ***p<0.001, NS, not significant.

(C) Expression of *cdh2* at 6hpf was measured by real-time quantitative PCR. Both *acvr1ba** and *sox32*-induced endodermal cells have elevated expression comparing to wild type uninjected controls. *p<0.05.

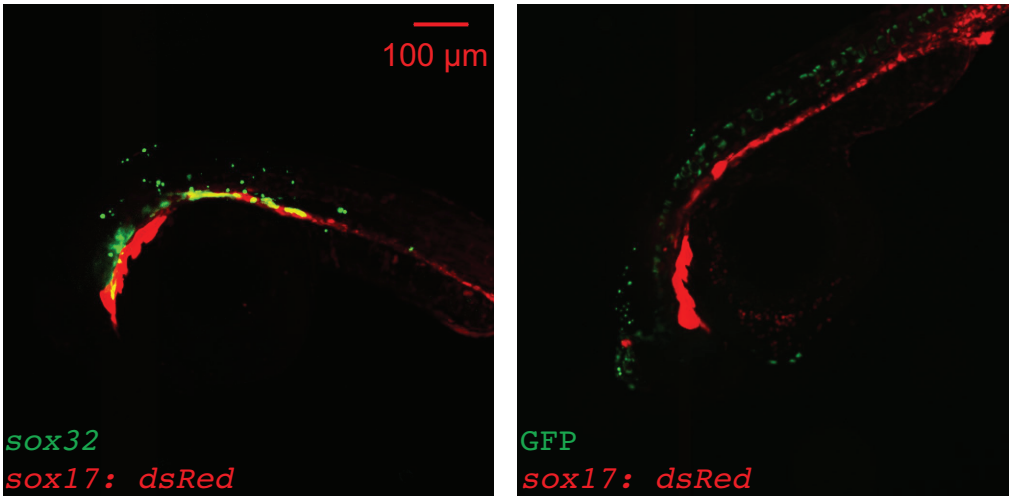

Figure S2: *sox32*-expressing cells preferentially segregate to endoderm-derived tissues when placed near the dorsal margin. Related to Figure 2.

Representative images showing distribution of *sox32*-overexpressing cells or GFP-expressing cells that were transplanted to the margin of wild-type host embryos. At 21-somite stage, transplanted *sox32*-overexpressing cells primarily localized to endodermal tissues while GFP-expressing cells localized to mesodermal tissues.

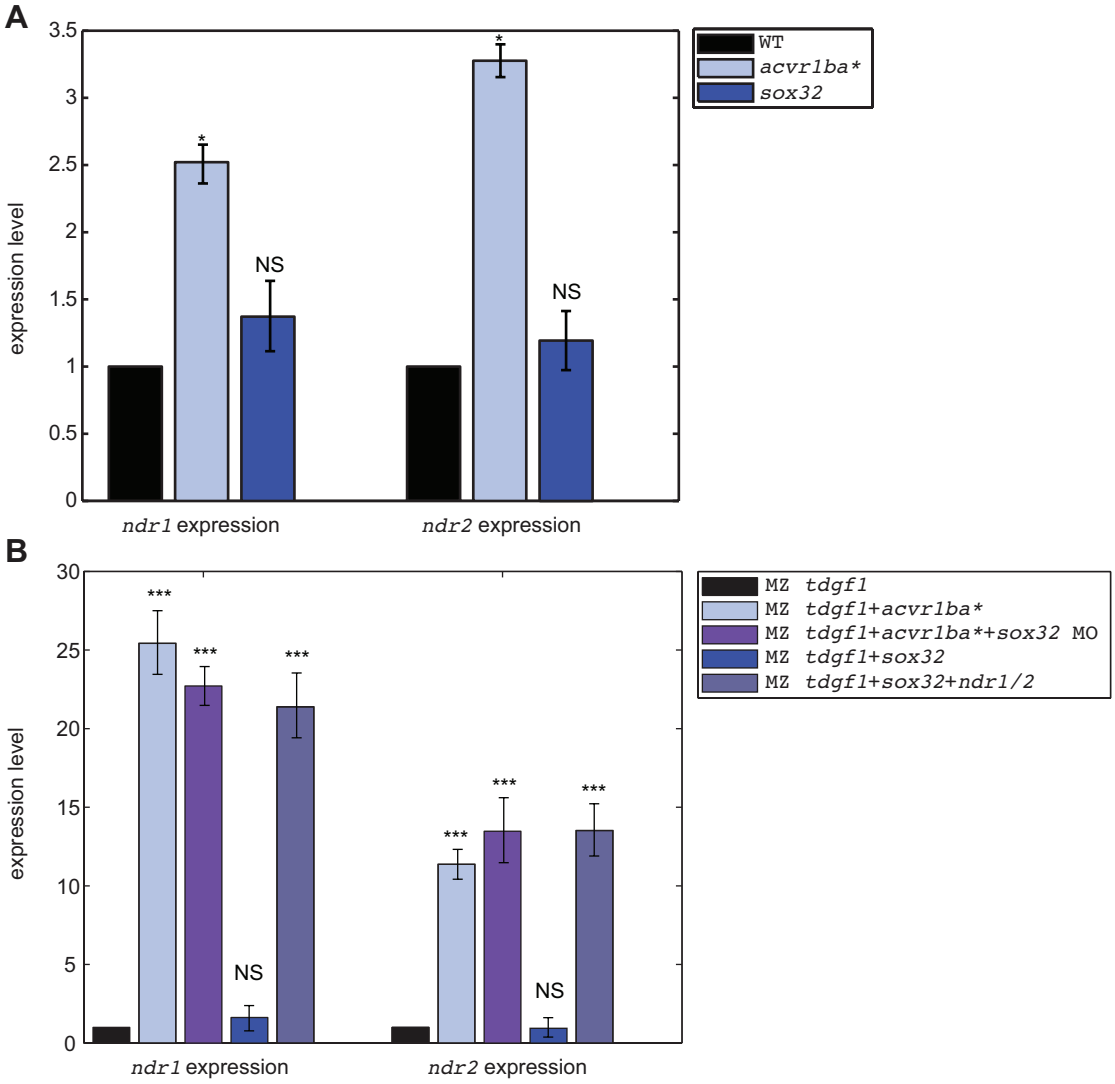

Figure S3: ***ndr1/2* is upregulated by *acvr1ba**, and *sox32* is neither necessary or sufficient for this upregulation. Related to Figure 2.**

(A) *ndr1/2* expression in *acvr1ba**-expressing cells and *sox32*-overexpressing cells in wildtype background measured by real-time quantitative PCR. *p<0.05, NS, not significant.

(B) *ndr1/2* expression under all experimental conditions in MZ *tdgf1* background, which removes the confounding effects of maternally deposited Ndr1/2 on driving nodal signaling. ***p<0.001, NS, not significant.

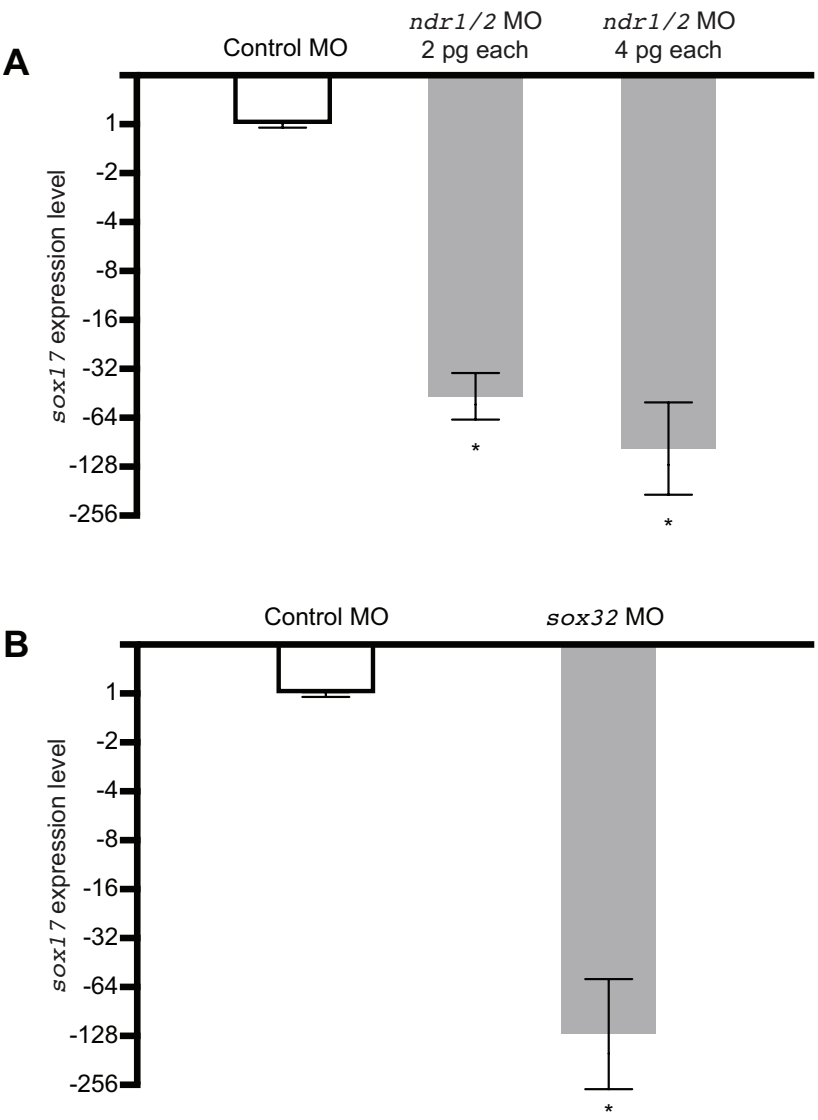

Figure S4: Validation of *ndr1*, *ndr2* and *sox32* morpholinos. Related to Figure 2.

(A) Validation of *ndr1/2* knockdown. Embryos were injected at the 1-cell stage with standard control (Gene Tools) or *ndr1* and *ndr2* MO. Total RNA was collected at 70% epiboly (7 hpf), and *sox17* expression was quantified by qPCR. ndr1/2 knockdown reduced *sox17* expression by 50-fold when 2pg each was injected and 80-fold when 4pg each was injected. Data represents averages of 3 biological replicates. Error bars, S.E.M. *p=0.01.

(B) Validation of *sox32* knockdown. Embryos were injected at the 1-cell stage with 2ng of standard control (Gene Tools) or *sox32* MO. Total RNA was collected at 70% epiboly (7 hpf), and *sox17* expression was quantified by qPCR. *sox32* knockdown reduced *sox17* expression by 125-fold. Data represents averages of 3 biological replicates. Error bars, S.E.M. *p=0.01.

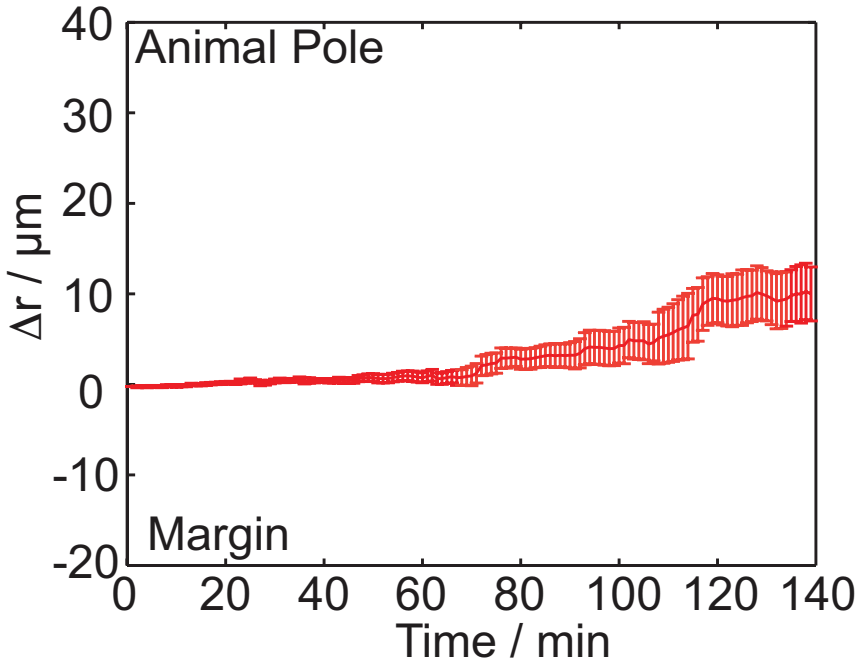

Figure S5: Single-cell tracking analysis of ingression of *acvr1ba-expressing cells with *sox32* MO. Related to Figure 2.**

Average relative distance with standard error plotted against time. Relative distance was calculated as in Fig. 2I. Unlike cells expressing *acvr1ba** only, cells also containing *sox32* MO move toward the surface of the embryo with their ectodermal neighbors.

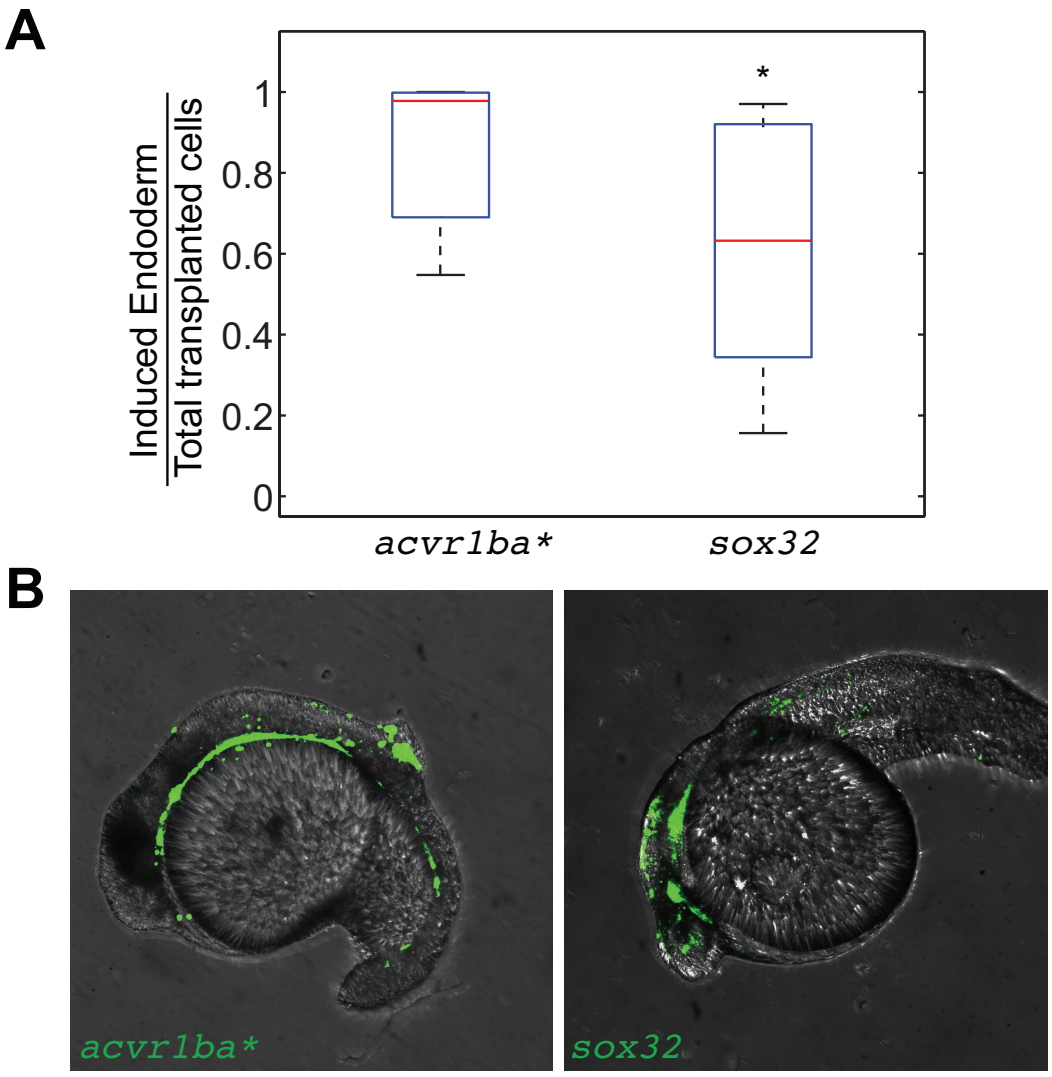

Figure S6: Induced endodermal cells internalize following transplantation to the margin.
(A) Boxplot quantification of endoderm contribution of transplanted cells at 18 hpf. Data is shown as mean ± SEM of independent transplantation experiments with 14 embryos per condition. Student's t-test was performed. * $p<0.05$.
(B) Representative image showing distribution of transplanted cells depicted in (A) at 18 hpf. *acvr1ba**-expressing cells localized to the endoderm-derived tissue (green). Cells overexpressing *sox32* localize to both endoderm and ectoderm-derived tissue. Lateral view, anterior to the left.

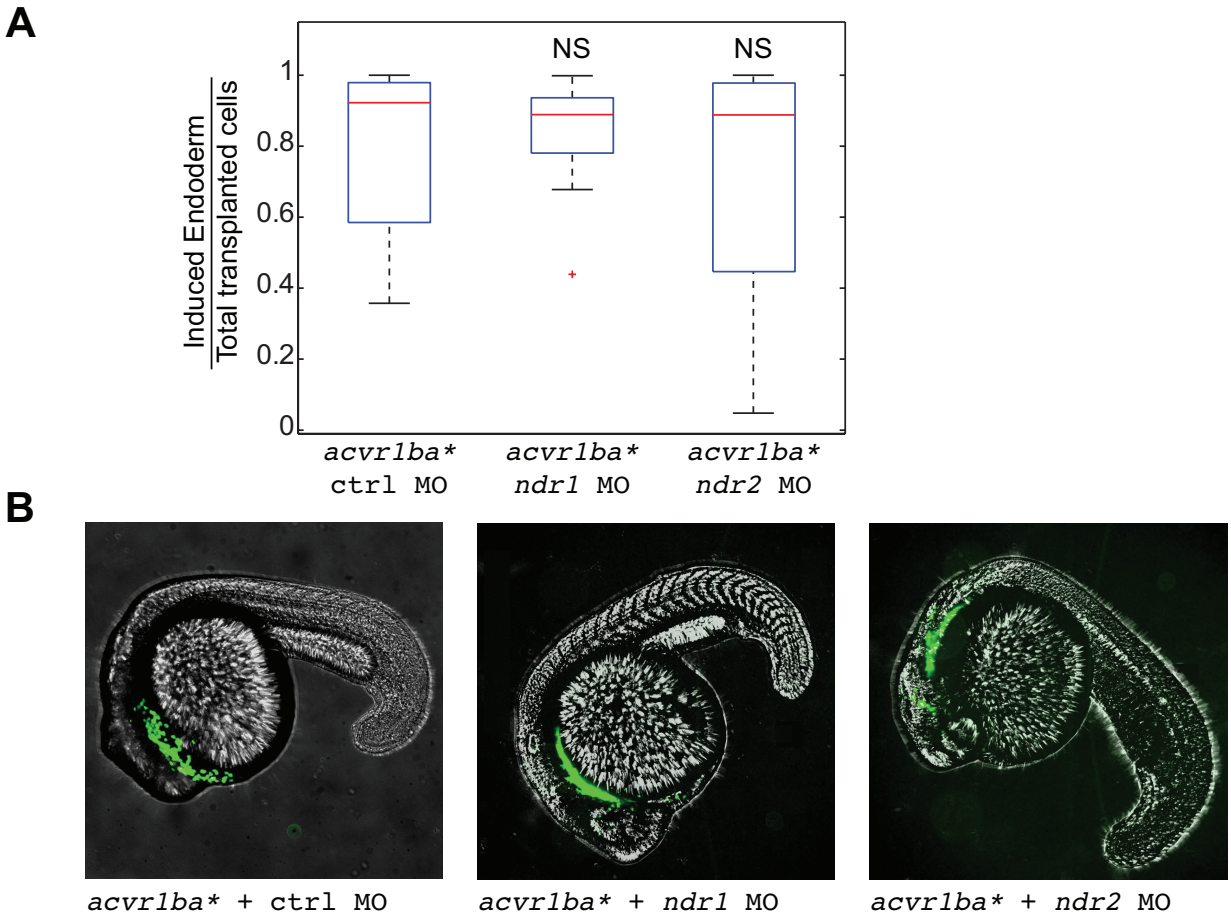

Figure S7: Ndr1 and Ndr2 act redundantly to support the ability of *acvr1ba cells to internalize.**

(A) Boxplot quantification of endoderm contribution of transplanted cells at 20 hpf. Data is shown as mean ± SEM of independent transplantation experiments with 16 embryos per condition. Student's t-test was performed. NS, not significant.

(B) Representative image showing distribution of transplanted cells depicted in (A) at 18 hpf. *acvr1ba**-expressing cells localized to the endoderm-derived tissue (green)in all three conditions, in contrast to the block of internalization when both Ndr1 and Ndr2 MO are combined in acvr1ba* cells (**Fig. 2H**). Lateral view, anterior to the left.

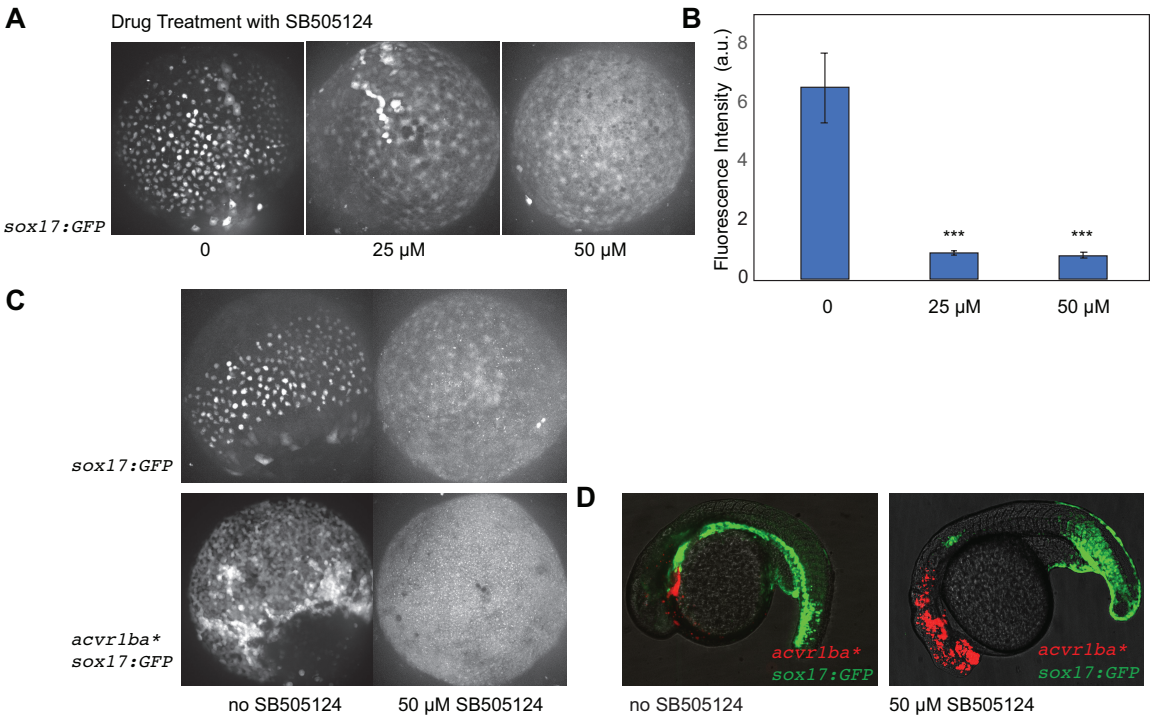

Figure S8: Nodal signaling inhibitor SB505124 blocks *acvr1ba-expressing cells from sorting.**

(A) Representative images of *sox17:GFP* expression under 0, 25 μM or 50 μM SB505124. Drug treatment began at 6 hpf, images were taken at 10 hpf. Animal pole view.

(B) Quantification of *sox17:GFP* fluorescence intensity under 0, 25 μM or 50 μM SB505124. *** p<0.001. n=3.

(C) *sox17:GFP* expression for embryos with or without injection of acvr1ba* and under no drug treatment or treated 50 μM drug SB505124 treatment.

(D) Transplant of *acvr1ba**-expressing cells into *sox17:GFP* background under DMSO control and 50 μM drug SB505124 treatment at 18hfp.

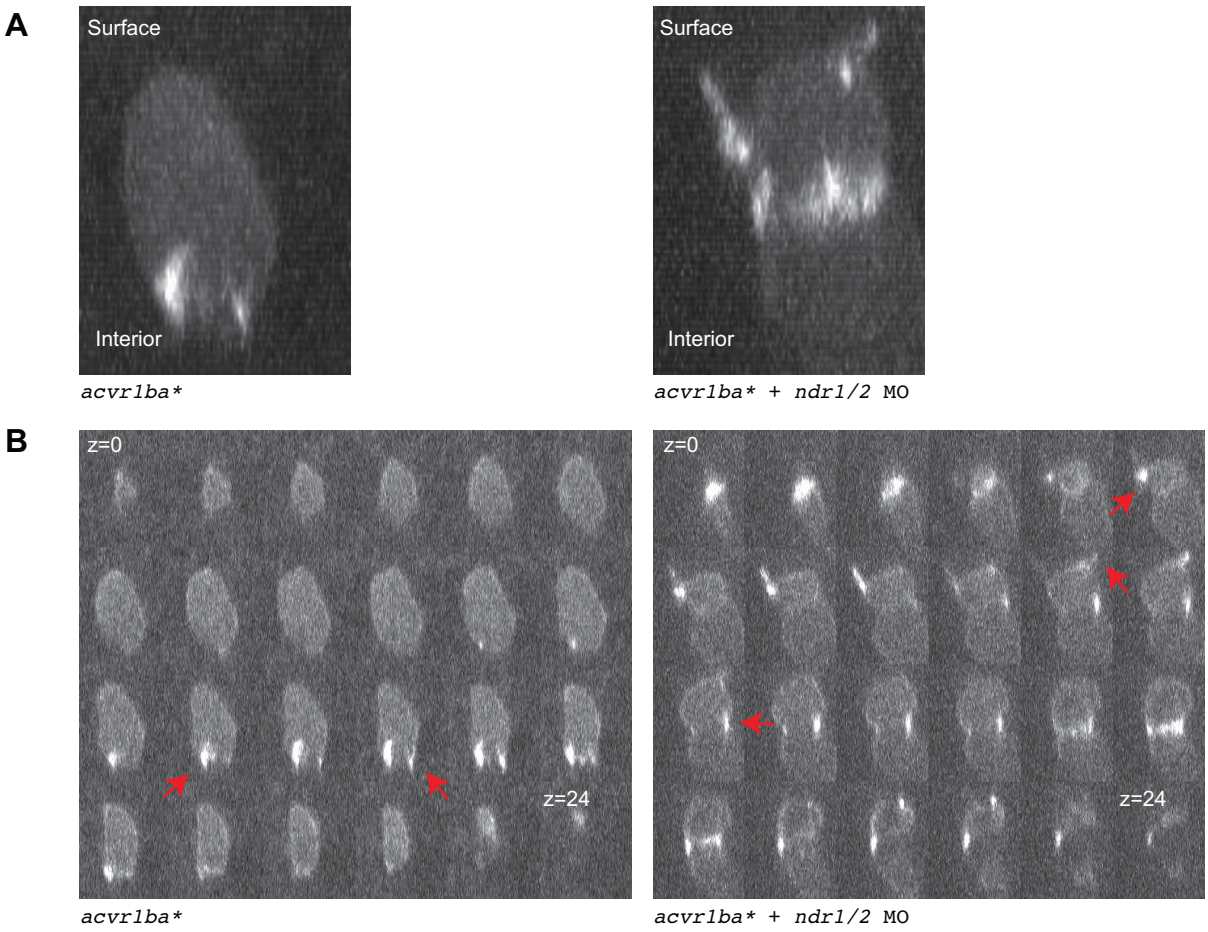

Figure S9: Blocking autocrine production of *ndr1/2* interferes with polarity of actin-based protrusions in *acvr1ba cells. Related to Figure 5.**

(A) Maximum? Z projection of individual transplanted cells injected with either *acvr1ba** alone or *acvr1ba** with *ndr1/2* MOs.

(B) Montage of Z stack of cells shown in (A). Red arrows indicate actin enrichment. Numbers indicate μm?

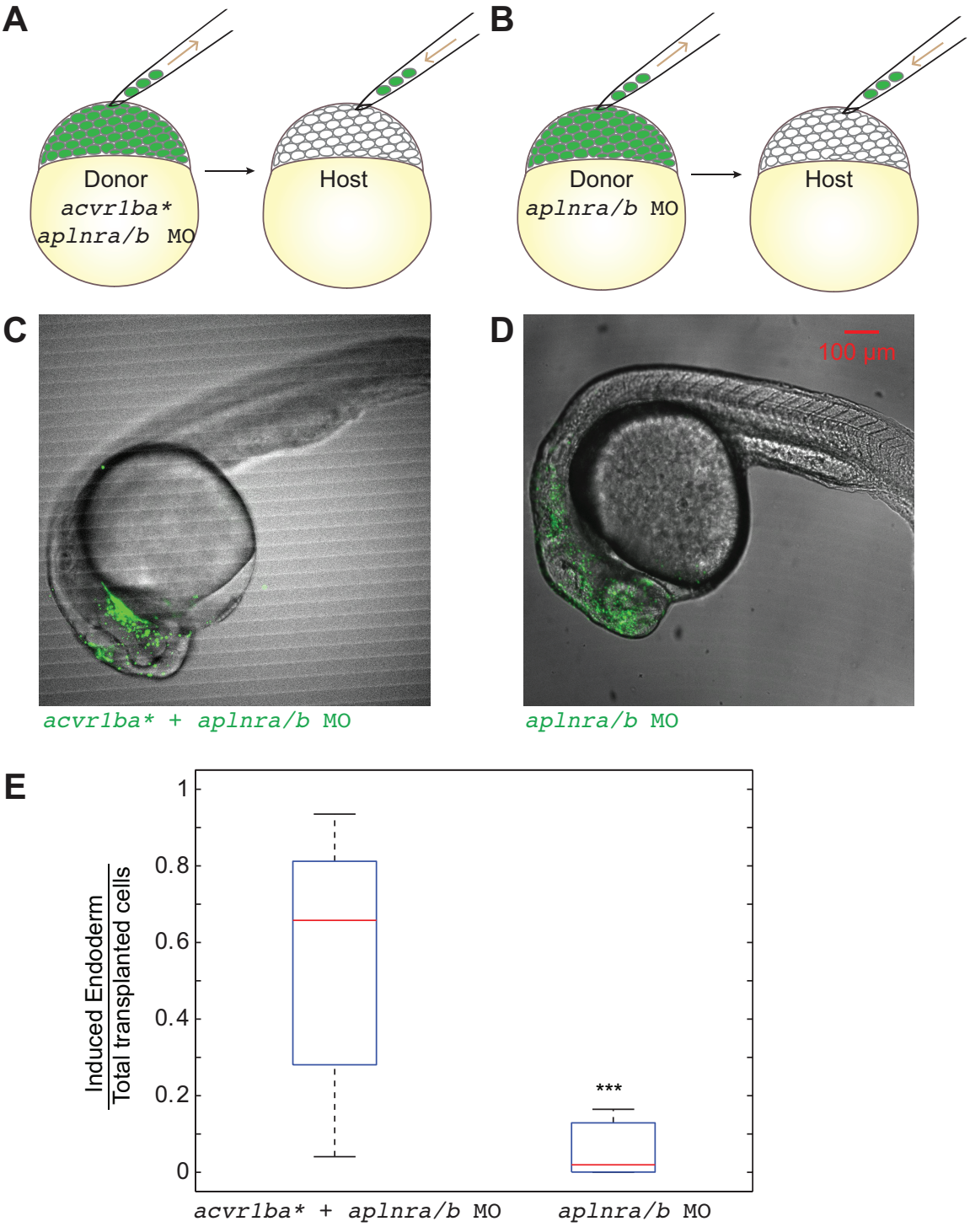

Figure S10: **Apelin receptor signaling is not essential for ectopic endoderm ingression.** **(A-B)** Schematic diagrams depicting single donor transplant assay to test the role of apelin receptor signaling. (A) *acvr1ba**-expressing cells with *aplnra* and *aplnrb* MOs were transplanted

to the animal pole of a wild-type host embryo. (B) Cells with *aplnra* and *aplnrb* MOs alone were transplanted to the animal pole of a wild-type host embryo.
(C-D) Representative images showing distribution of induced endodermal cells in a wild-type host. Donor cells in (A) (green) mainly localized to endoderm-derived tissue (C), while donor cells in (B) mainly localized to ectoderm-derived tissue (D). Lateral view, anterior to the right.
(E) Boxplot quantification of endoderm contribution at 21 hpf of transplanted cells depicted in (A-B). *acvr1ba**-expressing cells with *aplnra* and *aplnrb* MOs contributed to endoderm significantly more than cells with *aplnra* and *aplnrb* MOs alone. Data is shown as mean ± SEM of 3 independent transplantation experiments with 18 embryos per condition. Student's t-test was performed. *** $p<0.001$.

Table S1. List of Oligonucleotides

Oligonucleotide Name	Sequence
ef1a_forward	5′-CAAGAAGAGTAGTACCGCTAGCAT-3′
ef1a_reverse	5′-CACGGTGACAACATGCTGGAG-3′
sox17_forward	5'-CACAATGCGGAGCTGAGTAA-3'
sox17_reverse	5'-GCCTCCTCAACGAATGGAC-3'
sox32_forward	5'-CGGACCTGGAGAACACTGAC-3'
sox32_reverse	5'-GCATGTACGGACGCTTATCTG-3'
cdh2_forward	5'-CATCCCGGAGACATAGGAGA-3'
cdh2_reverse	5'-GCCCTCGTAGTCAAACACCA-3'
Oep5	5'-GAGATGGAGATGTTCTAATG-3'
Oep3m	5'-GAACAGTTGACTCGTCAC-3'
Oep3w	5'-GAACAGTTGACTCGTCAT-3'
Sox32 MO	5'-GCATCCGGTCGACATACATGCTGTT-3'
Sqt MO	5'-ATGTCAAATCAAGGTAATAATCCAC-3'
Cyc MO	5'-GCGACTCCCGAGCGTGTGCATGATG-3'
Aplnr a MO	5'-CGGTGTATTCCGGCGTTGGCTCCAT-3'
Aplnr b MO	5'-CAGAGAAGTTGTTTGTCATGTGCTC-3'
Control MO	5'-CCTCTTAACCTCAGTTACAATTTATA-3'

Table S2. Key Resource Table

Reagent or Resource	Source	Identifier
Chemicals, Peptides, and Recombinant Proteins		
Dextran, Alexa Fluor™ 647	Invitrogen	Cat#D22914

Dextran, Tetramethylrhodamine	Invitrogen	Cat#D1868
Dextran, Fluorescein	Invitrogen	Cat#D1821
Dextran, Alexa Fluor™ 680	Invitrogen	Cat#D34680
Histone H1 From Calf Thymus, Alexa Fluor™ 488 Conjugate	Invitrogen	Cat#H13188
Critical Commercial Assays		
mMESSAGE mMACHINE SP6 Transcription Kit	Ambion	Cat#AM1340
SuperScript VILO cDNA Synthesis Kit	Invitrogen	Cat#11754050
SYBR green PCR master mix	Applied Biosciences	Cat#4309155
Experimental Models: Organisms/Strains		
Zebrafish: AB/TL	This study	ZFIN: ZDB-GENO-960809-7
Zebrafish: EKW	This study	ZFIN: ZDB-GENO-031202-1
Zebrafish: Tg(sox17:GFP)	This study	ZFIN: ZDB-GENO-061228-1
Zebrafish: Tg(sox17:DsRed)	This study	ZFIN: ZDB-GENO-080812-1
Zebrafish: Tg(h2afva:h2afva-mCherry)	This study	ZFIN: ZDB-GENO-100923-1
Zebrafish: Tg(ubb:GFP-Smad2)	This study	N/A

Zebrafish: *tdgf1*$^{tz57/+}$	Lilianna Solnica-Krezel lab	ZFIN: ZDB-GENO-080708-1
Zebrafish: *tdgf1*$^{tz57/tz57}$	This study	ZFIN: ZDB-GENO-980202-989
Oligonucleotides		
List of oligonucleotides	See Table S1	N/A
Recombinant DNA		
pCS2-acbr1ba*	This study	N/A
pCS2-acbr1ba*-p2a-tBFP	This study	N/A
pCS2-sox32	This study	N/A
pCS2-sox32-p2a-tBFP	This study	N/A
pCS2-ndr1	This study	N/A
pCS2-ndr1-GFP	This study	N/A
pCS2-ndr2	This study	N/A
pCS2-ndr2-tBFP	This study	N/A
pCS2-GFP-UTRN	This study	N/A
pCS2-GFP	This study	N/A
pCS2-h2a-mCherry	This study	N/A
pCS2-tdgf1	This study	N/A
pmTol2-ef1a:Venus-Smad2	Steve Harvey	N/A
Software and Algorithms		

Fiji	NIH	https://fiji.sc
Matlab2013a	MathWorks Inc.	http://mathworks.com
TGMM	Philipp Keller lab	https://www.janelia.org/lab/keller-lab/software/fast-accurate-reconstruction-cell-lineages-large-scale-fluorescence

Contact for Reagent and Resource Sharing

Further information and requests for resources and reagents should be directed to Orion Weiner (orion.weiner@ucsf.edu).

Movie S1: *acvr1ba**-induced endodermal cells ingress into the inner layer when transplanted to the animal pole. Related to Figure 1. Frames were acquired every 5 min for 195 min. Playback is 7 frames/s.

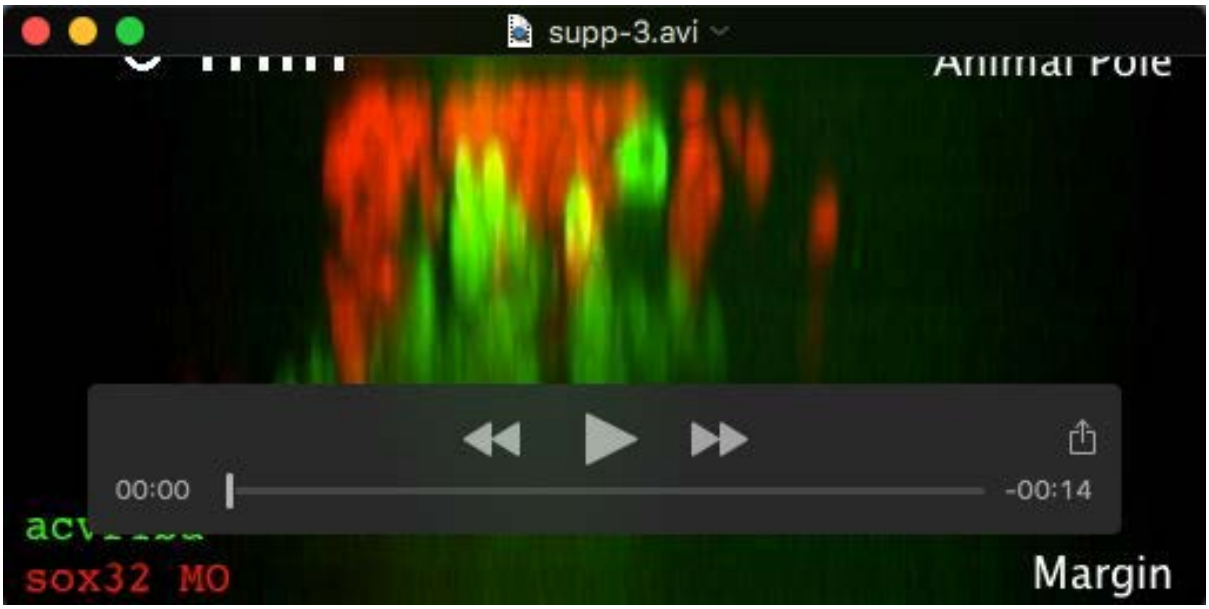

Movie S2: *acvr1ba**-induced endodermal cells and *sox32* MO induced ectodermal cells segregate into two separate layers. *sox32* MO-injected donor cells (red) remain on the outer layer of the embryo, while *acvr1ba**-injected donor cells (green) migrate into the inner layer of the embryo. Related to Figure 1. Frames were acquired every 3 min for 288 min. Playback is 7 frames/s.

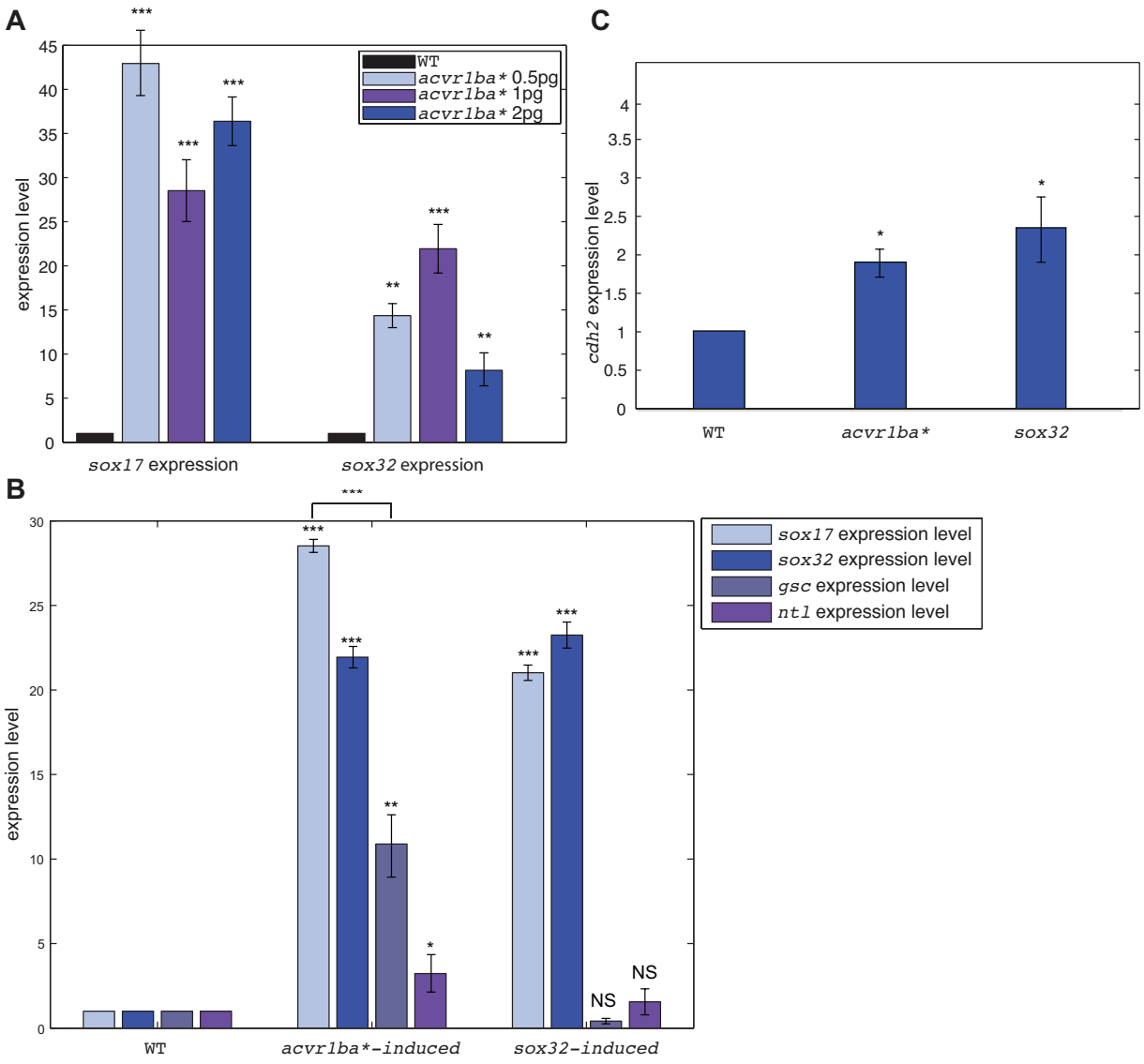

Figure S1: ***acvr1ba**** **induces expression of *sox17* and *sox32*. Related to Figure 1.**

(A) Expression of *sox17* and *sox32* endodermal markers was measured by real-time quantitative PCR. Constitutive activation of the Nodal pathway by expression of *acvr1ba** upregulated *sox17* and *sox32* expression (normalized to uninjected controls). **p<0.01, ***p<0.001.

(B) Expression of *sox17*, *sox32*, *gsc* and *ntl* was measured by real-time quantitative PCR in *acvr1ba**-expressing cells and *sox32*-expressing cells in wildtype background. Both acvrb1a* and sox32 more potently induce endodermal markers (*sox17* and *sox32*) than mesodermal markers (*gsc* and *ntl*). *p<0.05, **p<0.01, ***p<0.001, NS, not significant.

(C) Expression of *cdh2* at 6hpf was measured by real-time quantitative PCR. Both *acvr1ba** and *sox32*-induced endodermal cells have elevated expression comparing to wild type uninjected controls. *p<0.05.

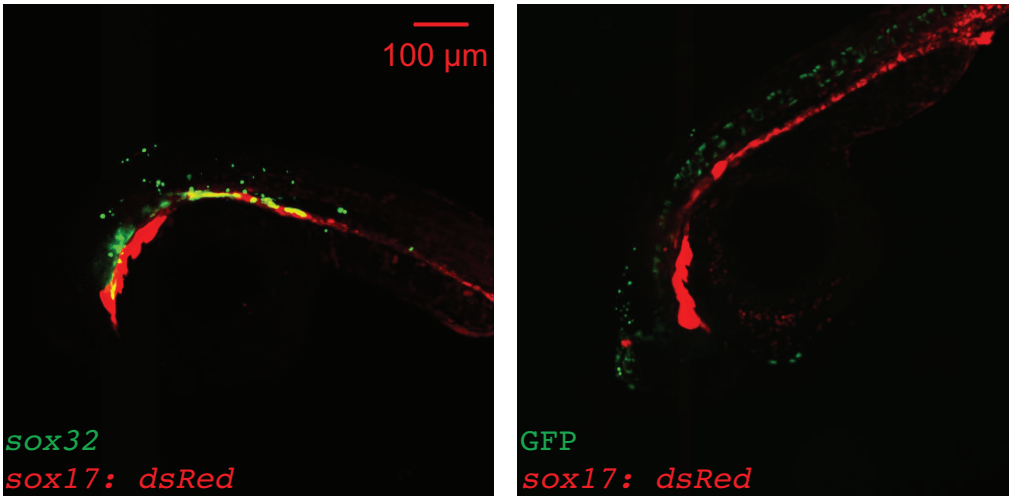

Figure S2: *sox32*-expressing cells preferentially segregate to endoderm-derived tissues when placed near the dorsal margin. Related to Figure 2.

Representative images showing distribution of *sox32*-overexpressing cells or GFP-expressing cells that were transplanted to the margin of wild-type host embryos. At 21-somite stage, transplanted *sox32*-overexpressing cells primarily localized to endodermal tissues while GFP-expressing cells localized to mesodermal tissues.

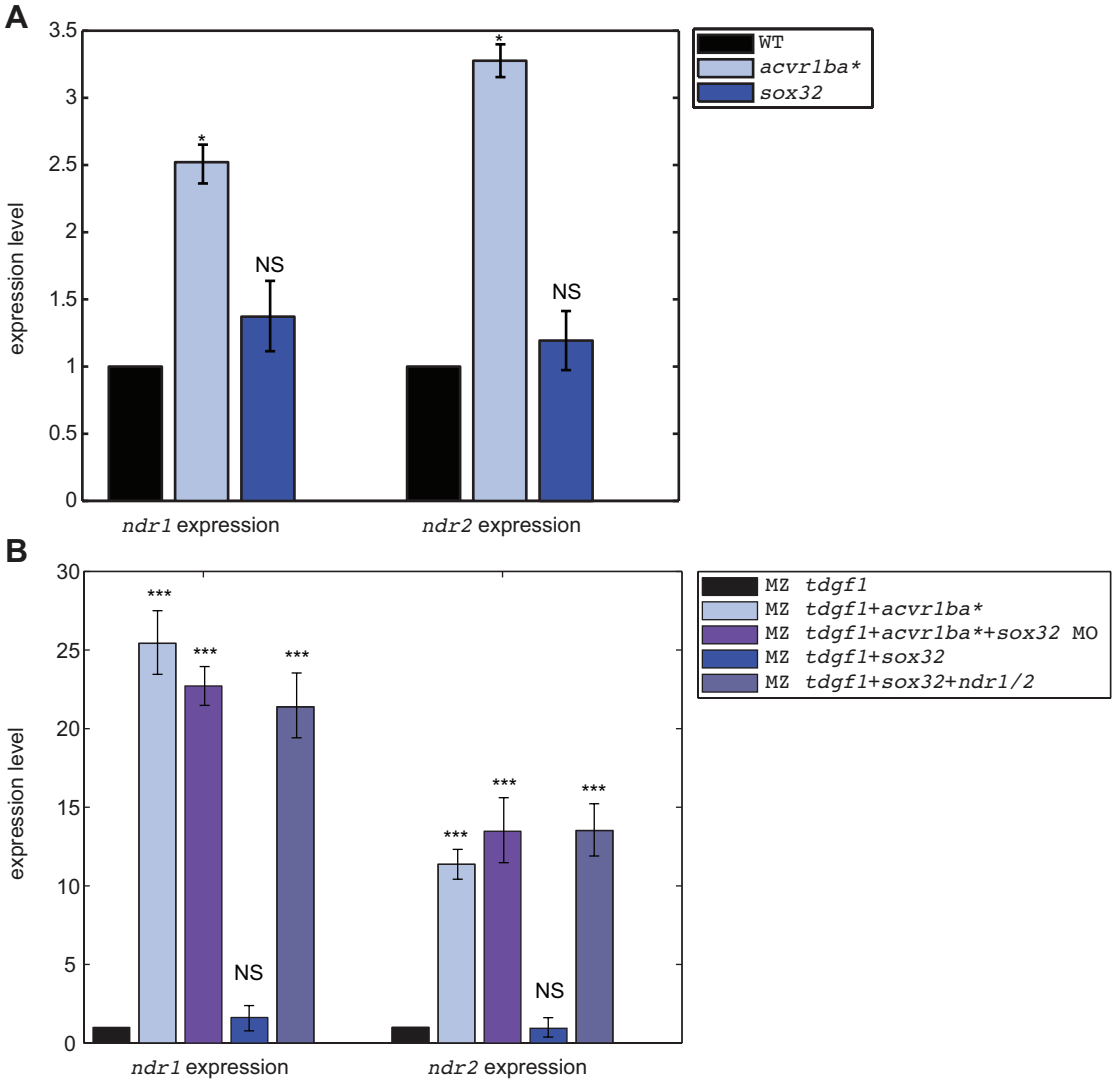

Figure S3: ***ndr1/2* is upregulated by *acvr1ba**, and *sox32* is neither necessary or sufficient for this upregulation. Related to Figure 2.**

(A) *ndr1/2* expression in *acvr1ba**-expressing cells and *sox32*-overexpressing cells in wildtype background measured by real-time quantitative PCR. *p<0.05, NS, not significant.

(B) *ndr1/2* expression under all experimental conditions in MZ *tdgf1* background, which removes the confounding effects of maternally deposited Ndr1/2 on driving nodal signaling. ***p<0.001, NS, not significant.

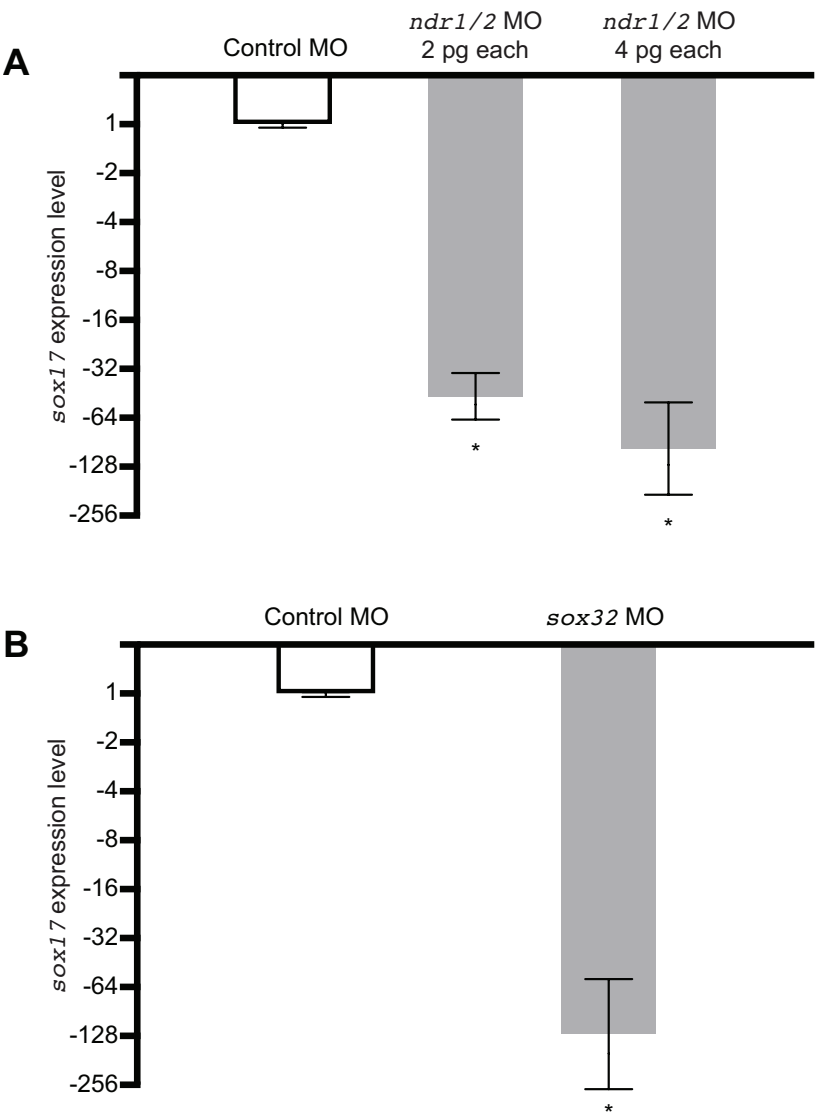

Figure S4: Validation of *ndr1*, *ndr2* and *sox32* morpholinos. Related to Figure 2.

(A) Validation of *ndr1/2* knockdown. Embryos were injected at the 1-cell stage with standard control (Gene Tools) or *ndr1* and *ndr2* MO. Total RNA was collected at 70% epiboly (7 hpf), and *sox17* expression was quantified by qPCR. ndr1/2 knockdown reduced *sox17* expression by 50-fold when 2pg each was injected and 80-fold when 4pg each was injected. Data represents averages of 3 biological replicates. Error bars, S.E.M. *p=0.01.

(B) Validation of *sox32* knockdown. Embryos were injected at the 1-cell stage with 2ng of standard control (Gene Tools) or *sox32* MO. Total RNA was collected at 70% epiboly (7 hpf), and *sox17* expression was quantified by qPCR. *sox32* knockdown reduced *sox17* expression by 125-fold. Data represents averages of 3 biological replicates. Error bars, S.E.M. *p=0.01.

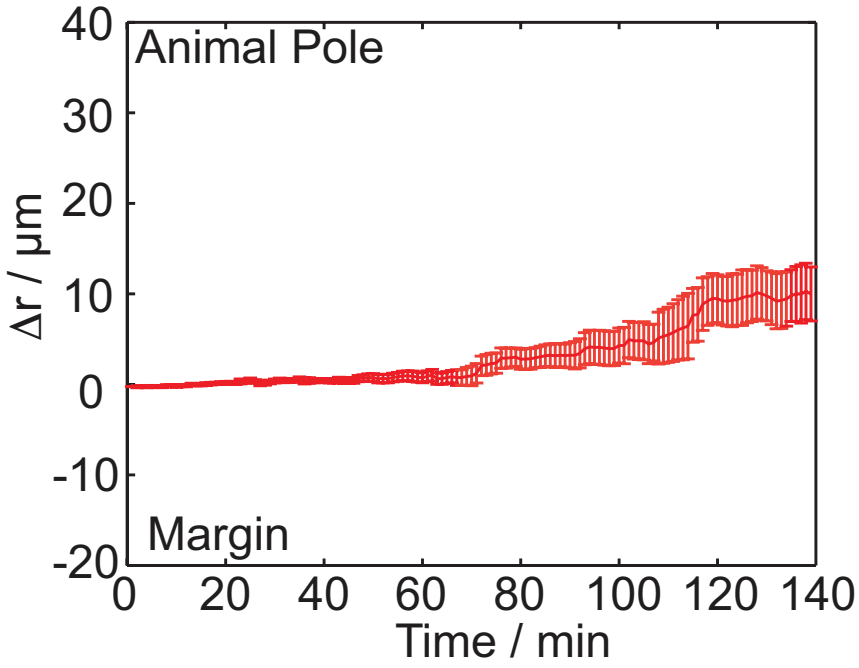

Figure S5: Single-cell tracking analysis of ingression of *acvr1ba-expressing cells with *sox32* MO. Related to Figure 2.**

Average relative distance with standard error plotted against time. Relative distance was calculated as in Fig. 2I. Unlike cells expressing *acvr1ba** only, cells also containing *sox32* MO move toward the surface of the embryo with their ectodermal neighbors.

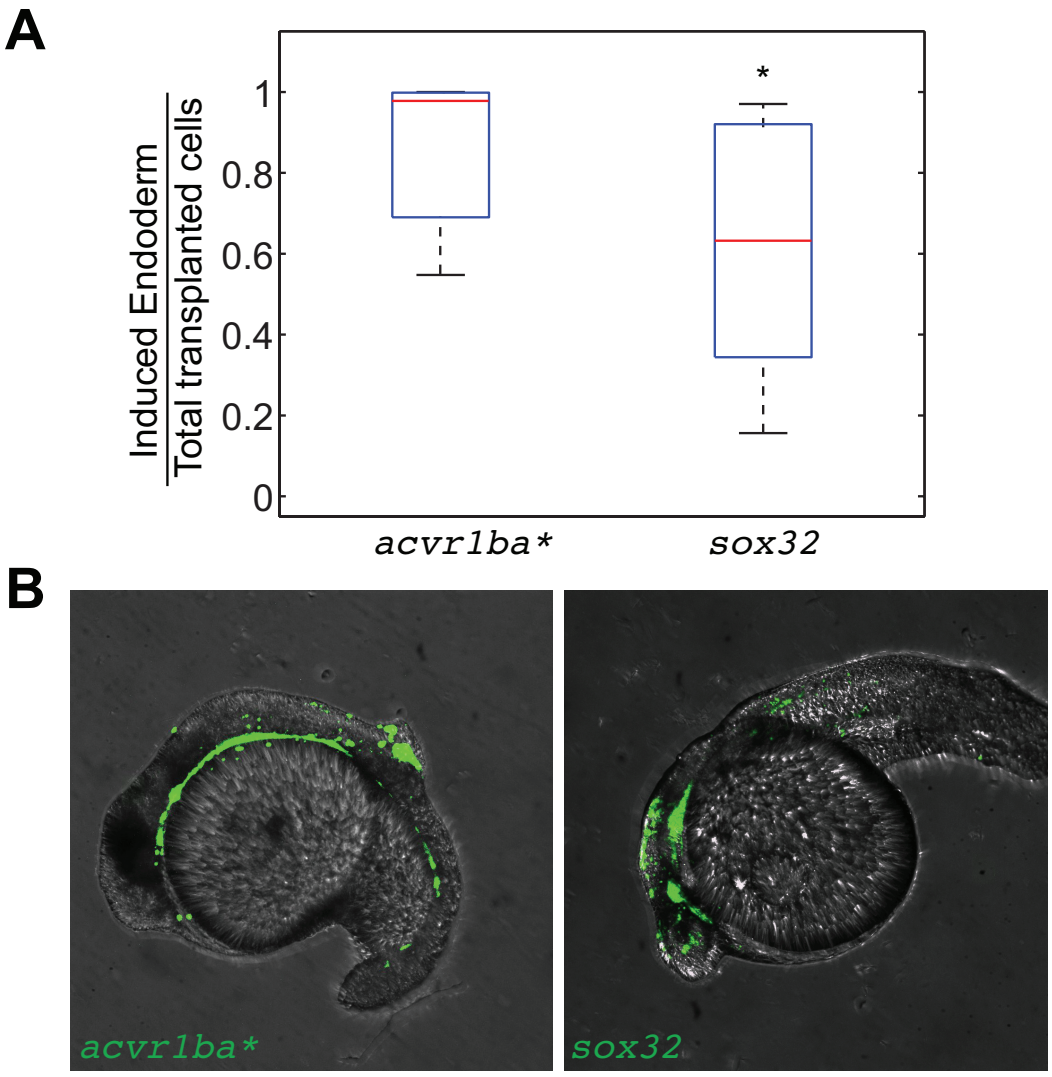

Figure S6: Induced endodermal cells internalize following transplantation to the margin.
(A) Boxplot quantification of endoderm contribution of transplanted cells at 18 hpf. Data is shown as mean ± SEM of independent transplantation experiments with 14 embryos per condition. Student's t-test was performed. * $p<0.05$.
(B) Representative image showing distribution of transplanted cells depicted in (A) at 18 hpf. *acvr1ba**-expressing cells localized to the endoderm-derived tissue (green). Cells overexpressing *sox32* localize to both endoderm and ectoderm-derived tissue. Lateral view, anterior to the left.

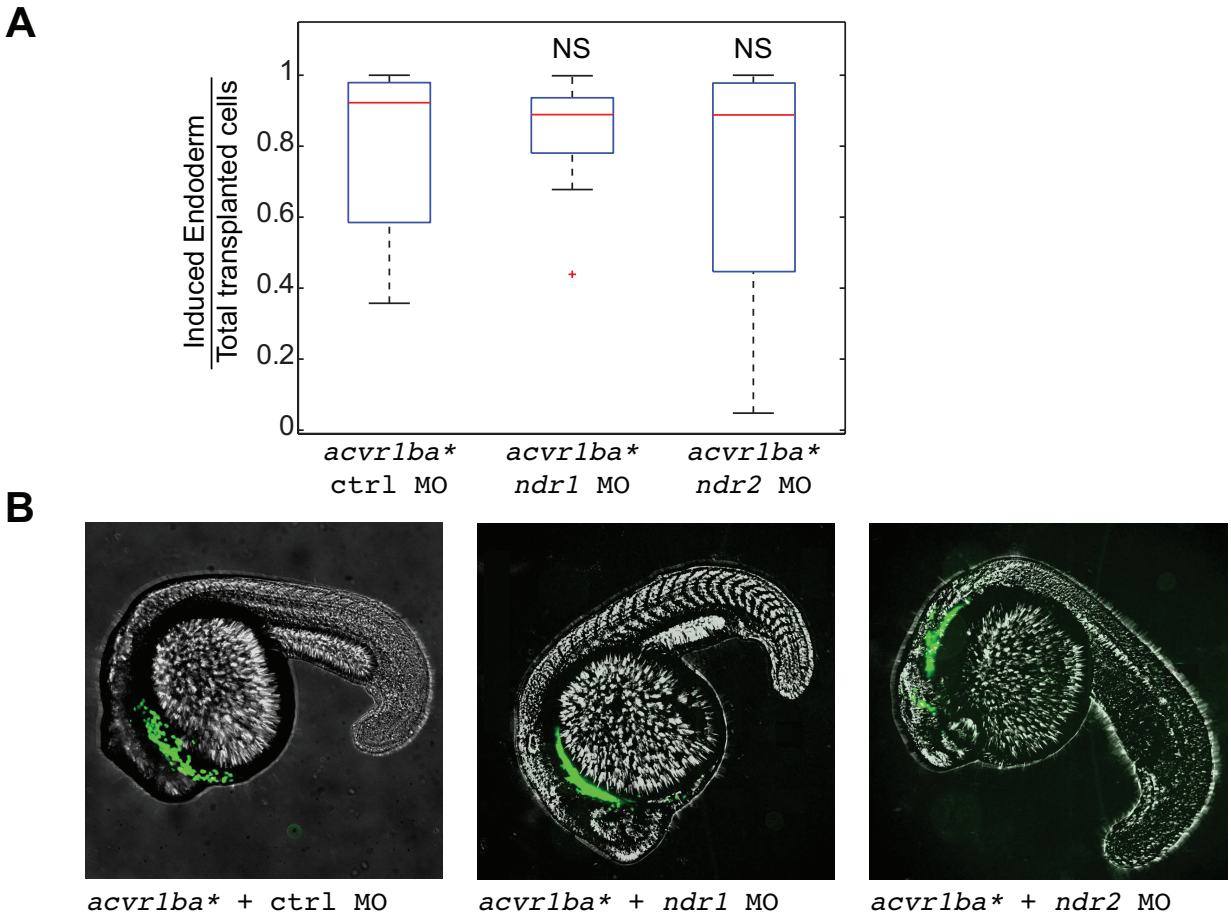

Figure S7: Ndr1 and Ndr2 act redundantly to support the ability of *acvr1ba cells to internalize.**

(A) Boxplot quantification of endoderm contribution of transplanted cells at 20 hpf. Data is shown as mean ± SEM of independent transplantation experiments with 16 embryos per condition. Student's t-test was performed. NS, not significant.

(B) Representative image showing distribution of transplanted cells depicted in (A) at 18 hpf. *acvr1ba**-expressing cells localized to the endoderm-derived tissue (green)in all three conditions, in contrast to the block of internalization when both Ndr1 and Ndr2 MO are combined in acvr1ba* cells (**Fig. 2H**). Lateral view, anterior to the left.

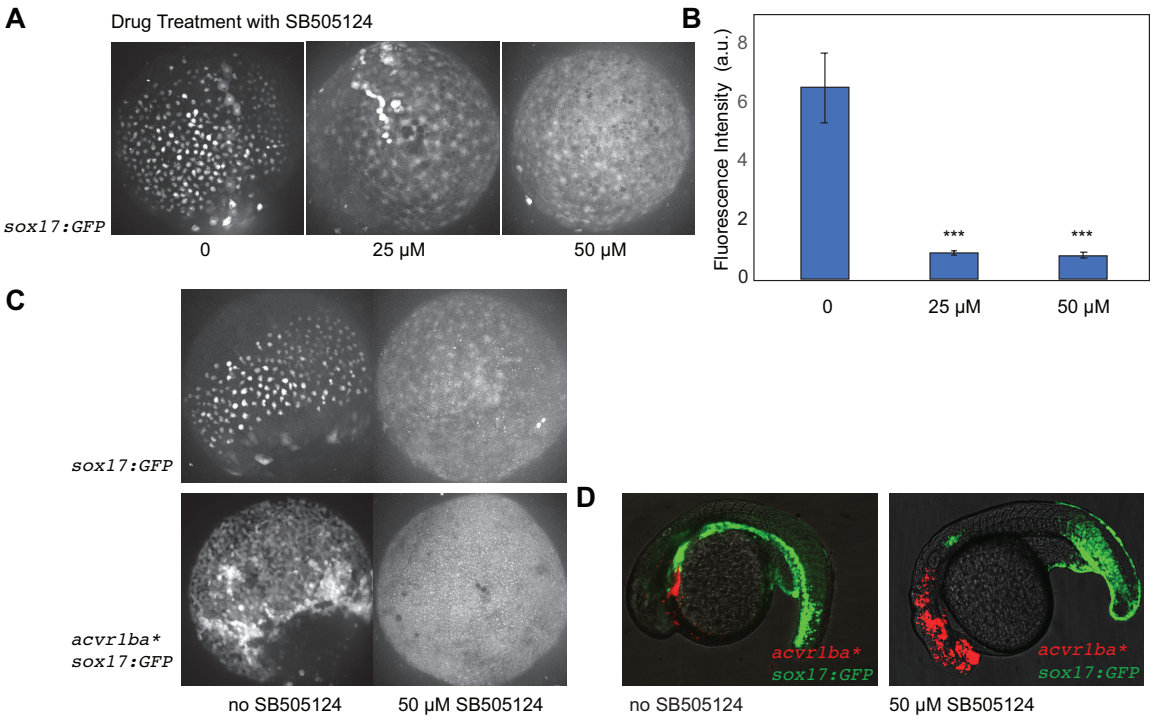

Figure S8: Nodal signaling inhibitor SB505124 blocks *acvr1ba-expressing cells from sorting.**

(A) Representative images of *sox17:GFP* expression under 0, 25 μM or 50 μM SB505124. Drug treatment began at 6 hpf, images were taken at 10 hpf. Animal pole view.

(B) Quantification of *sox17:GFP* fluorescence intensity under 0, 25 μM or 50 μM SB505124. *** p<0.001. n=3.

(C) *sox17:GFP* expression for embryos with or without injection of acvr1ba* and under no drug treatment or treated 50 μM drug SB505124 treatment.

(D) Transplant of *acvr1ba**-expressing cells into *sox17:GFP* background under DMSO control and 50 μM drug SB505124 treatment at 18hfp.

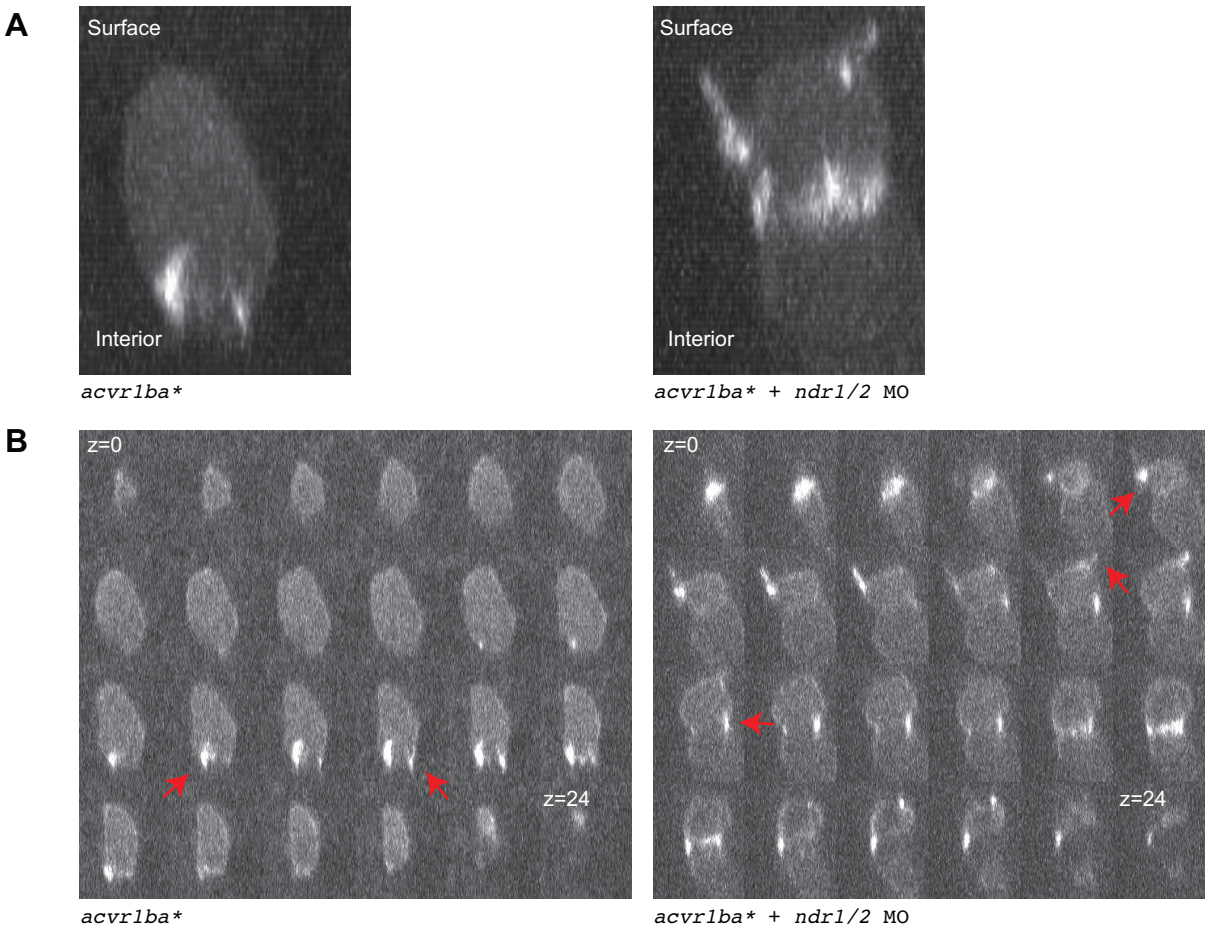

Figure S9: Blocking autocrine production of *ndr1/2* interferes with polarity of actin-based protrusions in *acvr1ba cells. Related to Figure 5.**

(A) Maximum? Z projection of individual transplanted cells injected with either *acvr1ba** alone or *acvr1ba** with *ndr1/2* MOs.

(B) Montage of Z stack of cells shown in (A). Red arrows indicate actin enrichment. Numbers indicate μm?

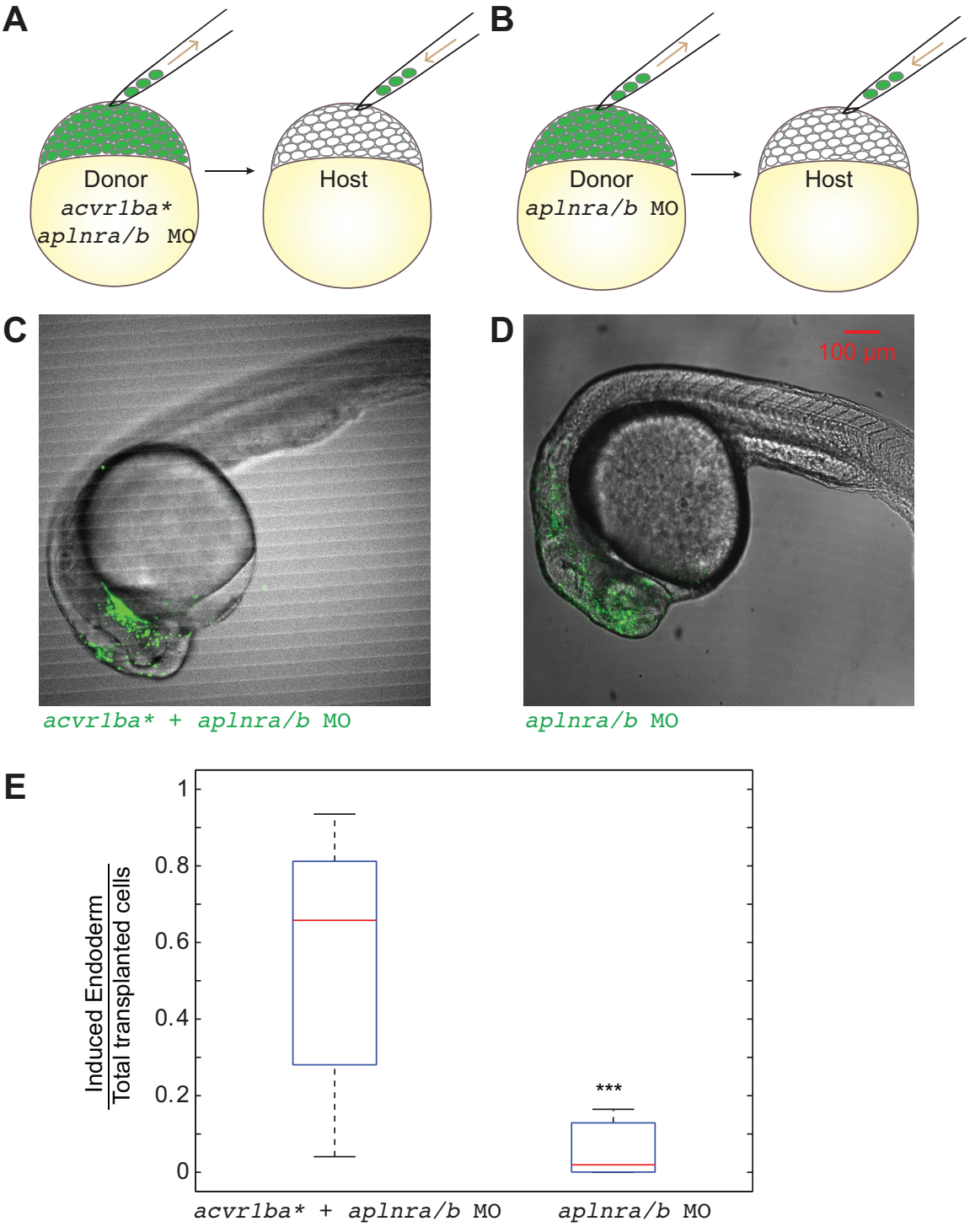

Figure S10: **Apelin receptor signaling is not essential for ectopic endoderm ingression.** **(A-B)** Schematic diagrams depicting single donor transplant assay to test the role of apelin receptor signaling. (A) *acvr1ba**-expressing cells with *aplnra* and *aplnrb* MOs were transplanted

to the animal pole of a wild-type host embryo. (B) Cells with *aplnra* and *aplnrb* MOs alone were transplanted to the animal pole of a wild-type host embryo.
(C-D) Representative images showing distribution of induced endodermal cells in a wild-type host. Donor cells in (A) (green) mainly localized to endoderm-derived tissue (C), while donor cells in (B) mainly localized to ectoderm-derived tissue (D). Lateral view, anterior to the right.
(E) Boxplot quantification of endoderm contribution at 21 hpf of transplanted cells depicted in (A-B). *acvr1ba**-expressing cells with *aplnra* and *aplnrb* MOs contributed to endoderm significantly more than cells with *aplnra* and *aplnrb* MOs alone. Data is shown as mean ± SEM of 3 independent transplantation experiments with 18 embryos per condition. Student's t-test was performed. *** $p<0.001$.

Table S1. List of Oligonucleotides

Oligonucleotide Name	Sequence
ef1a_forward	5′-CAAGAAGAGTAGTACCGCTAGCAT-3′
ef1a_reverse	5′-CACGGTGACAACATGCTGGAG-3′
sox17_forward	5'-CACAATGCGGAGCTGAGTAA-3'
sox17_reverse	5'-GCCTCCTCAACGAATGGAC-3'
sox32_forward	5'-CGGACCTGGAGAACACTGAC-3'
sox32_reverse	5'-GCATGTACGGACGCTTATCTG-3'
cdh2_forward	5'-CATCCCGGAGACATAGGAGA-3'
cdh2_reverse	5'-GCCCTCGTAGTCAAACACCA-3'
Oep5	5'-GAGATGGAGATGTTCTAATG-3'
Oep3m	5'-GAACAGTTGACTCGTCAC-3'
Oep3w	5'-GAACAGTTGACTCGTCAT-3'
Sox32 MO	5'-GCATCCGGTCGACATACATGCTGTT-3'
Sqt MO	5'-ATGTCAAATCAAGGTAATAATCCAC-3'
Cyc MO	5'-GCGACTCCCGAGCGTGTGCATGATG-3'
Aplnr a MO	5'-CGGTGTATTCCGGCGTTGGCTCCAT-3'
Aplnr b MO	5'-CAGAGAAGTTGTTTGTCATGTGCTC-3'
Control MO	5'-CCTCTTAACCTCAGTTACAATTTATA-3'

Table S2. Key Resource Table

Reagent or Resource	Source	Identifier
Chemicals, Peptides, and Recombinant Proteins		
Dextran, Alexa Fluor™ 647	Invitrogen	Cat#D22914

Dextran, Tetramethylrhodamine	Invitrogen	Cat#D1868
Dextran, Fluorescein	Invitrogen	Cat#D1821
Dextran, Alexa Fluor™ 680	Invitrogen	Cat#D34680
Histone H1 From Calf Thymus, Alexa Fluor™ 488 Conjugate	Invitrogen	Cat#H13188
Critical Commercial Assays		
mMESSAGE mMACHINE SP6 Transcription Kit	Ambion	Cat#AM1340
SuperScript VILO cDNA Synthesis Kit	Invitrogen	Cat#11754050
SYBR green PCR master mix	Applied Biosciences	Cat#4309155
Experimental Models: Organisms/Strains		
Zebrafish: AB/TL	This study	ZFIN: ZDB-GENO-960809-7
Zebrafish: EKW	This study	ZFIN: ZDB-GENO-031202-1
Zebrafish: Tg(sox17:GFP)	This study	ZFIN: ZDB-GENO-061228-1
Zebrafish: Tg(sox17:DsRed)	This study	ZFIN: ZDB-GENO-080812-1
Zebrafish: Tg(h2afva:h2afva-mCherry)	This study	ZFIN: ZDB-GENO-100923-1
Zebrafish: Tg(ubb:GFP-Smad2)	This study	N/A

Zebrafish: *tdgf1*$^{tz57/+}$	Lilianna Solnica-Krezel lab	ZFIN: ZDB-GENO-080708-1
Zebrafish: *tdgf1*$^{tz57/tz57}$	This study	ZFIN: ZDB-GENO-980202-989
Oligonucleotides		
List of oligonucleotides	See Table S1	N/A
Recombinant DNA		
pCS2-acbr1ba*	This study	N/A
pCS2-acbr1ba*-p2a-tBFP	This study	N/A
pCS2-sox32	This study	N/A
pCS2-sox32-p2a-tBFP	This study	N/A
pCS2-ndr1	This study	N/A
pCS2-ndr1-GFP	This study	N/A
pCS2-ndr2	This study	N/A
pCS2-ndr2-tBFP	This study	N/A
pCS2-GFP-UTRN	This study	N/A
pCS2-GFP	This study	N/A
pCS2-h2a-mCherry	This study	N/A
pCS2-tdgf1	This study	N/A
pmTol2-ef1a:Venus-Smad2	Steve Harvey	N/A
Software and Algorithms		

Fiji	NIH	https://fiji.sc
Matlab2013a	MathWorks Inc.	http://mathworks.com
TGMM	Philipp Keller lab	https://www.janelia.org/lab/keller-lab/software/fast-accurate-reconstruction-cell-lineages-large-scale-fluorescence

Contact for Reagent and Resource Sharing

Further information and requests for resources and reagents should be directed to Orion Weiner (orion.weiner@ucsf.edu).

Movie S1: *acvr1ba**-induced endodermal cells ingress into the inner layer when transplanted to the animal pole. Related to Figure 1. Frames were acquired every 5 min for 195 min. Playback is 7 frames/s.

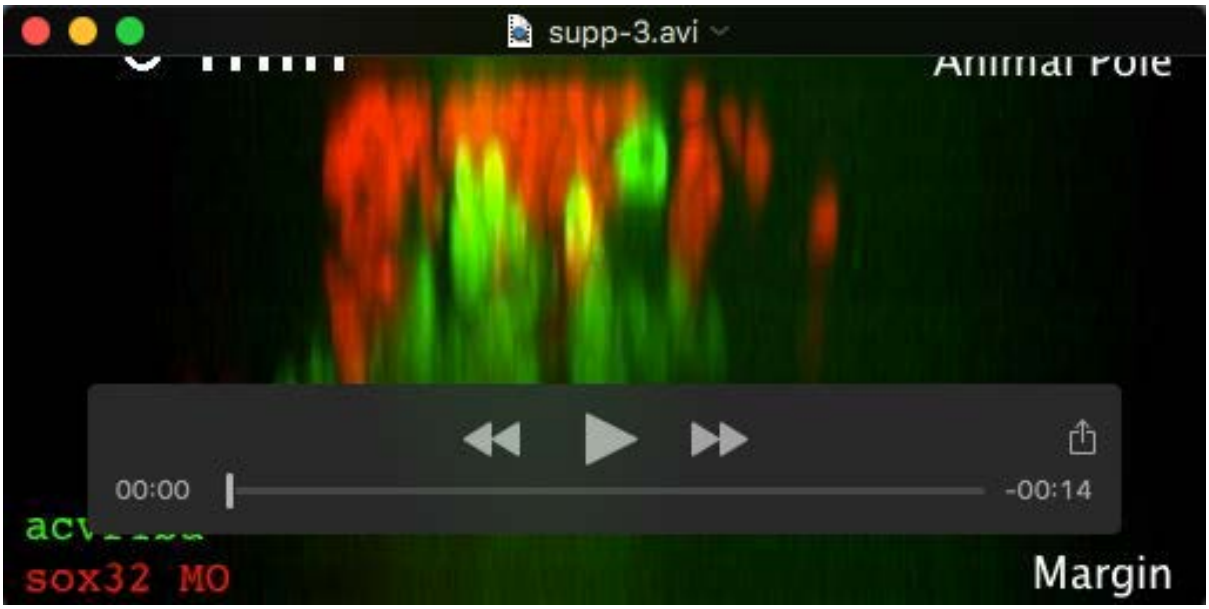

Movie S2: *acvr1ba**-induced endodermal cells and *sox32* MO induced ectodermal cells segregate into two separate layers. *sox32* MO-injected donor cells (red) remain on the outer layer of the embryo, while *acvr1ba**-injected donor cells (green) migrate into the inner layer of the embryo. Related to Figure 1. Frames were acquired every 3 min for 288 min. Playback is 7 frames/s.